Downloaded from rsta.royalsocietypublishing.org

PHILOSOPHICAL TRANSACTIONS OF THE ROYAL SOCIETY A
MATHEMATICAL, PHYSICAL & ENGINEERING SCIENCES

Surface-Specific Analytical Techniques

J. C. Riviere

Phil. Trans. R. Soc. Lond. A 1982 **305**, 545-589
doi: 10.1098/rsta.1982.0051

Email alerting service

Receive free email alerts when new articles cite this article - sign up in the box at the top right-hand corner of the article or click **here**

To subscribe to *Phil. Trans. R. Soc. Lond. A* go to: **http://rsta.royalsocietypublishing.org/subscriptions**

This journal is © 1982 The Royal Society

Downloaded from rsta.royalsocietypublishing.org

MATHEMATICAL, PHYSICAL & ENGINEERING SCIENCES
THE ROYAL SOCIETY A
PHILOSOPHICAL TRANSACTIONS OF

Phil. Trans. R. Soc. Lond. A **305**, 545–589 (1982)
Printed in Great Britain

Surface-specific analytical techniques

By J. C. Rivière
Materials Development Division, Atomic Energy Research Establishment, Harwell, Didcot, Oxon. OX11 0RA, U.K.

CONTENTS

Introduction

Electron excitation
- Auger electron spectroscopy
- Scanning Auger microscopy
- Electron energy-loss spectroscopy
- Appearance potential spectroscopy
- Electron-induced luminescence
- Electron-stimulated desorption

Photon excitation
- X-ray photoelectron spectroscopy
- X-ray excited Auger electron spectroscopy
- Synchrotron radiation photoelectron spectroscopy
- Ultraviolet photoelectron spectroscopy
- Photoelectron spectromicroscopy
- Ellipsometry

Ion excitation
- Ion-excited Auger electron spectroscopy
- Proton-excited Auger electron spectroscopy
- Ion neutralization spectroscopy
- Ion beam spectrochemical analysis
- Glow discharge optical spectroscopy
- Static secondary ion mass spectrometry
- Ion scattering spectroscopy
- Glow discharge mass spectrometry

Resolution and sensitivity

Conclusions

References

MATHEMATICAL, PHYSICAL & ENGINEERING SCIENCES
THE ROYAL SOCIETY A
PHILOSOPHICAL TRANSACTIONS OF

The Royal Society is collaborating with JSTOR to digitize, preserve, and extend access to *Philosophical Transactions of the Royal Society of London. Series A, Mathematical and Physical Sciences.* STOR® www.jstor.org

Downloaded from rsta.royalsocietypublishing.org

Many new surface analytical techniques have appeared over the last few years, and their proliferation has led to some confusion about what sort of information is provided by each, and what is the appropriate field of application. In this paper those techniques that are surface-specific are described and discussed, i.e. those that give information about the surface only, the surface in this context being the first few atom layers, extending to about 5 nm. The coverage is restricted to those techniques providing elemental or chemical analysis, or both, so that structural techniques are excluded. They are grouped according to the method of initial excitation, i.e. electron, photon or ion, and where appropriate comparisons will be made to emphasize their respective advantages and disadvantages.

Introduction

In recent years the number of techniques that can be used to characterize surfaces has been increasing steadily, and so has the variety of information available about the chemical and physical properties of surfaces. The proliferation is such that some confusion may exist among those not working in the field about what type of information is provided by each technique, and what are the respective advantages and disadvantages of one against another. In this paper only those techniques that are concerned with elemental and chemical analysis of surfaces will be described and discussed; those that give structural information, such as l.e.e.d. and r.h.e.e.d., will be excluded on the grounds that they really need separate treatment. Since the 'surface', in this context, will be taken to mean the first few atom layers, extending to approximately 5 nm, the techniques described will be those that are inherently surface-specific, i.e. in which only the surface is analysed.

In table 1 the surface-specific techniques are listed by their acronyms, a guide to which is given. The list may not be exhaustive; new techniques and variations on existing ones appear frequently, and by the time this paper is published it is likely that the list should be extended. As can be seen, the techniques can be arranged as a matrix in which the columns refer to the nature of the primary excitation and the rows to the emitted particles or radiation whose measurement provides the information. It is convenient during discussion to consider the techniques in groups according to the primary excitation used, and that will be the method adopted here. For other recent reviews on this subject, the reader is referred to Larrabee (1977), Morgan & Werner (1978), Holloway & McGuire (1978), Evans & Blattner (1978), and to Holloway & McGuire (1981).

Electron excitation

Auger electron spectroscopy (*A.e.s.*)

A beam of primary electrons of energy chosen in the range 5–20 keV impinges on a surface and causes ionization of core levels in atoms at and near the surface. The ionized atoms relax either by emission of an X-ray photon of characteristic energy or by ejection of an Auger electron via a two-electron process, but for shallow core levels of binding energies less than *ca.* 2000 eV the Auger process predominates. The energy range of Auger electrons normally covered is from 20 to 1000 eV, and figure 1, from Seah & Dench (1978), shows that if electrons in that kinetic energy range are to escape from the surface without losing energy by scattering then they must originate within *ca.* 1.5 nm of the surface.

For each element there is a unique set of Auger energies, since no two atoms have the same set of binding energies, and therefore elemental identification at the surface is possible. Some

Downloaded from rsta.royalsocietypublishing.org

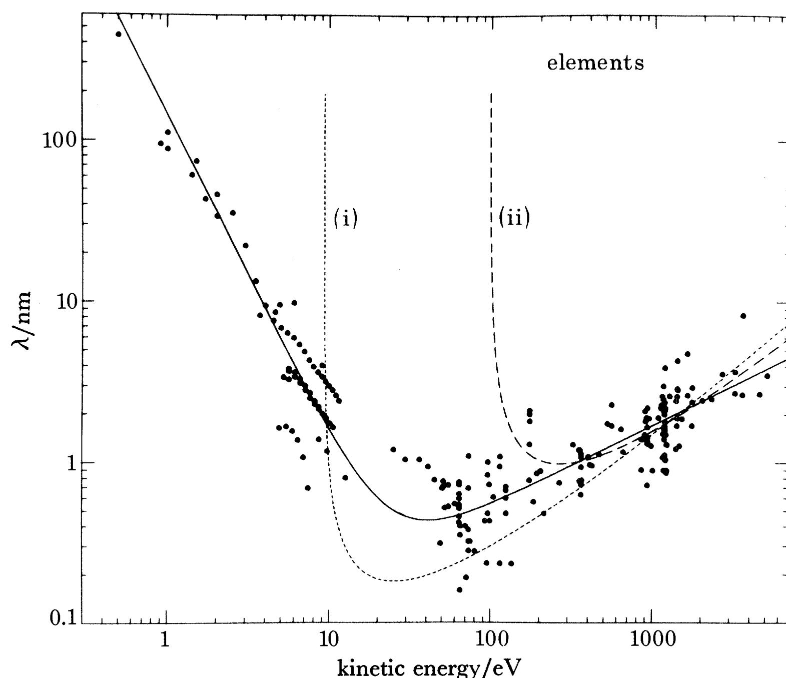

FIGURE 1. The compilation by Seah & Dench (1979) of measurements of the inelastic mean free path (corresponding closely to the average escape depth), as a function of kinetic energy. The full line is an empirical least squares fit, and the broken curves (i) and (ii) are theoretical predictions.

TABLE 1. MATRIX OF SURFACE-SPECIFIC ANALYTICAL TECHNIQUES

excitation... / emission	electrons	photons	ions
electrons	A.e.s. s.a.m. e.e.l.s.	X.p.s. X.A.e.s. s.r.p.s. u.p.s. p.e.s.m.	i.A.e.s. p.A.e.s. i.n.s.
photons	a.p.s. e.i.l.	ellipsometry	i.b.s.c.a. g.d.o.s.
ions	e.s.d.	—	s.s.i.m.s. i.s.s. g.d.m.s.

List of abbreviations

A.e.s.	Auger electron spectroscopy
s.A.m.	scanning Auger microscopy
e.e.l.s.	electron energy-loss spectroscopy
a.p.s.	appearance potential spectroscopy (= s.X.a.p.s.)
e.i.l.	electron-induced luminescence
e.s.d.	electron-stimulated desorption
X.p.s.	X-ray photoelectron spectroscopy (= e.s.c.a.)
X.A.e.s.	X-ray (excited) Auger electron spectroscopy
s.r.p.s.	synchrotron radiation photoelectron spectroscopy
u.p.s.	ultraviolet photoelectron spectroscopy
p.e.s.m.	photoelectron spectromicroscopy
i.A.e.s.	ion (excited) Auger electron spectroscopy
p.A.e.s.	proton (excited) Auger electron spectroscopy
i.n.s.	ion neutralization spectroscopy
i.b.s.c.a.	ion beam spectrochemical analysis (=s.c.a.n.i.i.r.)
g.d.o.s.	glow discharge optical spectrometry
s.s.i.m.s.	static secondary ion mass spectrometry
i.s.s.	ion-scattering spectroscopy
g.d.m.s.	glow discharge mass spectrometry

Downloaded from rsta.royalsocietypublishing.org

typical Auger spectra, recorded as the differential of the secondary electron energy distribution, are shown in figure 2, for some transition metals. In this example, from Weber (1972), the three major peaks, based on LMM Auger transitions, are characteristic of the elements from Sc to Zn. The relative magnitudes of the three peaks change progressively, an indication of the changes in the valence band population through the series, since two of the peaks in the triplet involve electrons from the valence band.

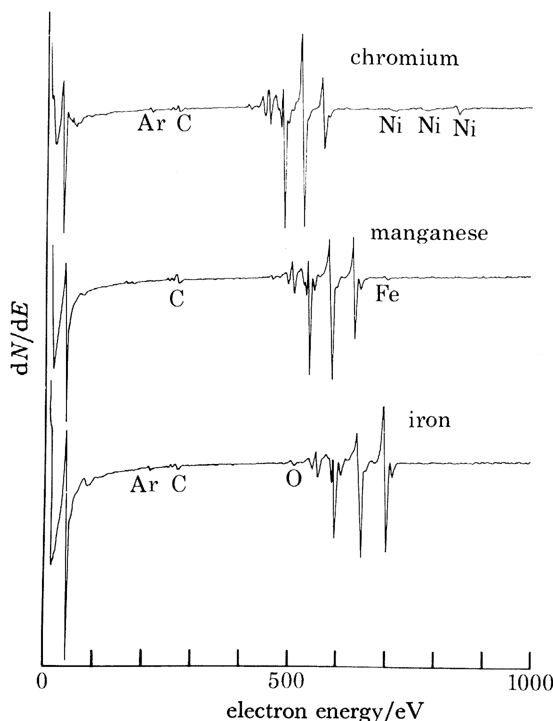

FIGURE 2. Electron-excited LMM Auger spectra of three transition metals. The major triplet of peaks is characteristic of the first transition series, and can be seen repeated from the nickel impurity in the chromium. The large peak at low energies, *ca.* 50 eV in each case, is the $M_{2,3}$ VV Auger peak. The carbon KVV peak is just visible in each spectrum, from contamination on the surface, while on two of the metals there is enough embedded argon from the cleaning procedure to give rise to the argon $L_{2,3}$ VV Auger peak. (From Weber (1972).)

Some chemical information is also available from A.e.s. The Auger spectra of non-metallic elements can show marked differences from one compound to another, and can thus be used in an empirical 'fingerprinting' manner to identify chemical state. More detailed information of a chemical nature is beginning to emerge from a careful study of the line shapes of Auger peaks based on transitions involving valence band electrons. Figure 3, for example, from the work of Jennison *et al.* (1981), compares the carbon KVV Auger spectrum from various metal carbonyls and from gaseous CO; the additional strong feature at *ca.* 260 eV in the carbonyl spectra can be shown to be due to initial-state π back-bonding. Properly applied deconvolution procedures can also provide knowledge about the local density of electronic states around individual atoms and therefore about the nature of the bonding between surface atoms and those immediately below them.

Downloaded from rsta.royalsocietypublishing.org

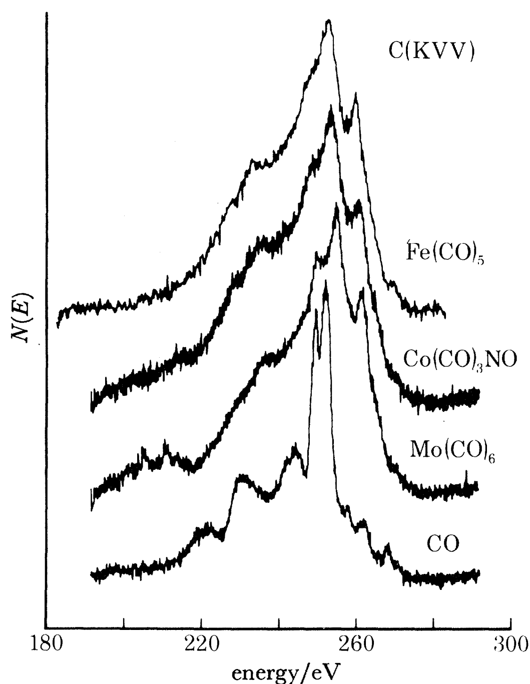

FIGURE 3. Comparison by Jennison *et al.* (1981) of the carbon KVV Auger spectrum from various metal carbonyls with that from CO, showing the presence of chemical information in the carbonyl spectra. The large feature seen at about 260 eV could be shown to be due to π back-bonding from the CO to the nickel.

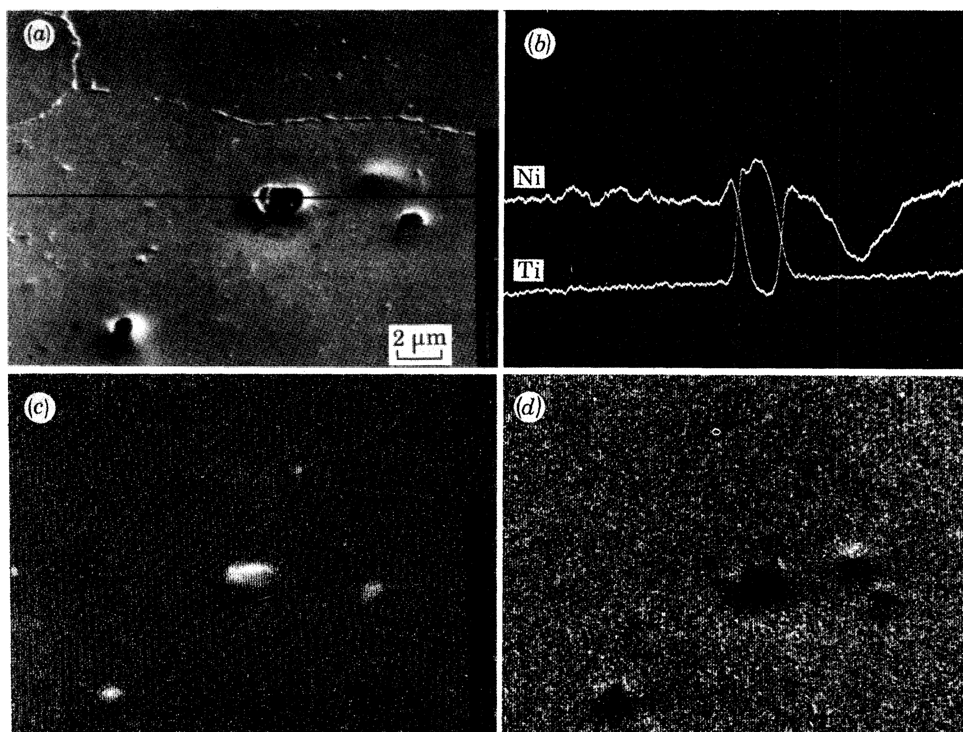

FIGURE 4. Analysis by s.A.m. of an inclusion in the surface of polished and etched Nimonic PE16. (*a*) Secondary electron image with line of analysis; (*b*) Auger line analysis through the inclusion, showing a deficiency of nickel and an excess of titanium, based on selected LMM peaks; (*c*) Auger map with the use of the titanium LMM signal; (*d*) Auger map with the use of the nickel LMM signal. Spot analyses of the inclusions confirmed that they consisted mostly of TiC. (From Mogami (1979).)

PHILOSOPHICAL TRANSACTIONS OF THE ROYAL SOCIETY A MATHEMATICAL, PHYSICAL & ENGINEERING SCIENCES

PHILOSOPHICAL TRANSACTIONS OF THE ROYAL SOCIETY A MATHEMATICAL, PHYSICAL & ENGINEERING SCIENCES

Downloaded from rsta.royalsocietypublishing.org

PHILOSOPHICAL TRANSACTIONS OF THE ROYAL SOCIETY A MATHEMATICAL, PHYSICAL & ENGINEERING SCIENCES

Scanning Auger microscopy (*s.A.m.*)

Since electron beams can be focused into a very small area, and since there is in several fields, e.g. semiconductors and metallurgical fracture, a need to analyse ever smaller areas, one of the general trends in A.e.s. has been to finer and finer probe sizes. Because of electron optical design restraints, the reduction in probe size has had to be accompanied by a reduction in beam current and an increase in beam voltage, so that the state of the art at the moment in a high spatial resolution instrument would be that of a probe of diameter 50 nm formed from a beam of current about 1 nA and voltage about 35 kV. Electrons are easily deflected and so it has been a logical step from conventional A.e.s. to raster the primary beam at speeds up to television rates,

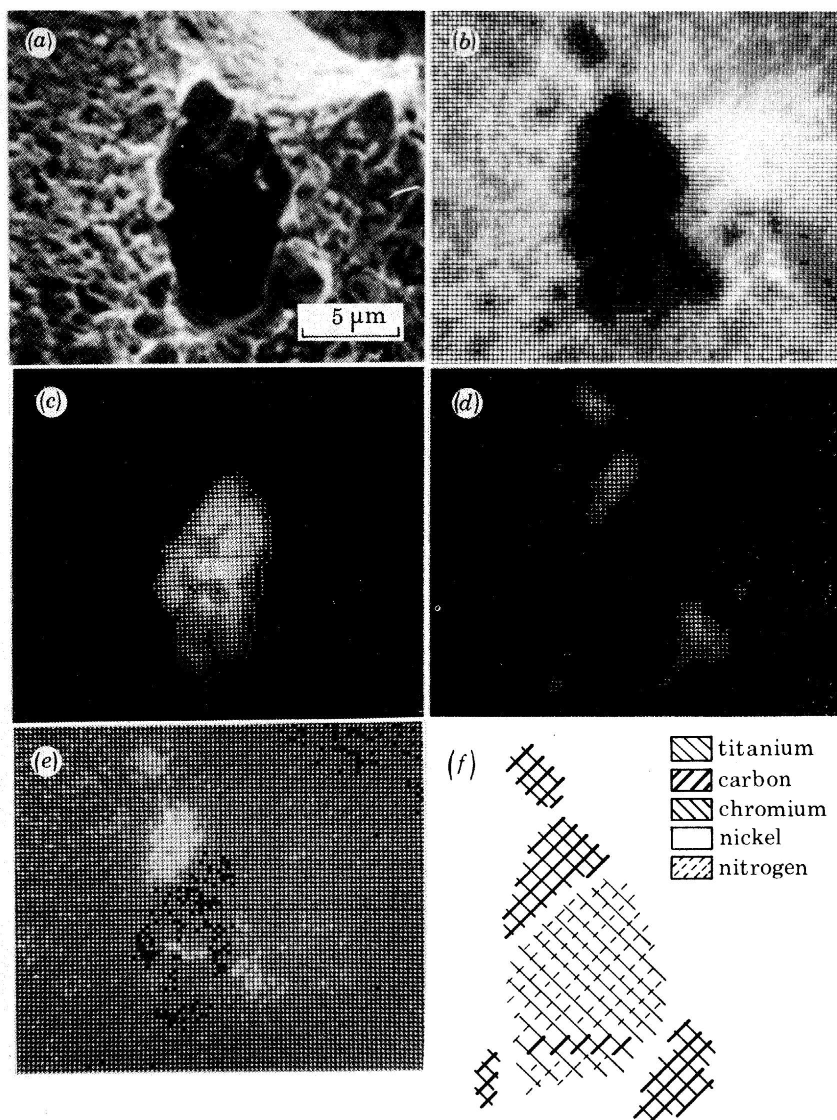

FIGURE 5. S.A.m. analysis of a particle found on the surface of a grain boundary exposed by intergranular fracture of a Nimonic 80A specimen: (*a*) secondary electron image; (*b*) Ni(836 eV); (*c*) Ti (373 eV); (*d*) Cr (518 eV); (*e*) C (272 eV). The maps have been computer enhanced to improve the contrast. Superposition of the maps gives (*f*), where it can be seen that part of the particle is chromium carbide, part titanium nitride, and the rest titanium carbide. (From Allen & Wild (1981).)

PHILOSOPHICAL TRANSACTIONS OF THE ROYAL SOCIETY A MATHEMATICAL, PHYSICAL & ENGINEERING SCIENCES

Downloaded from rsta.royalsocietypublishing.org

MATHEMATICAL, PHYSICAL & ENGINEERING SCIENCES
PHILOSOPHICAL TRANSACTIONS OF THE ROYAL SOCIETY A

and produce images either from the low-energy secondary electrons for topographical purposes (as in an s.e.m.) or from a selected Auger signal for elemental distribution across a surface. The latter technique, or variation of A.e.s., is called scanning Auger microscopy, or s.A.m. An example of its application is shown in figure 4, from Mogami (1979), in which a particle on an alloy surface has been analysed. Both line scans across the particle, and the elemental maps, show that it is rich in Ti but deficient in Ni.

Another application, in fractography, has been demonstrated by Allen & Wild (1981). In figure 5, a particle on a fracture face of Nimonic 80A has been selected for analysis. The s.A.m. maps show that it contains Ni, Ti, Cr and C, and by correlation it can be established which element goes with which, so that some areas of it can be seen to be chromium carbide, others titanium nitride, and a further small area titanium carbide.

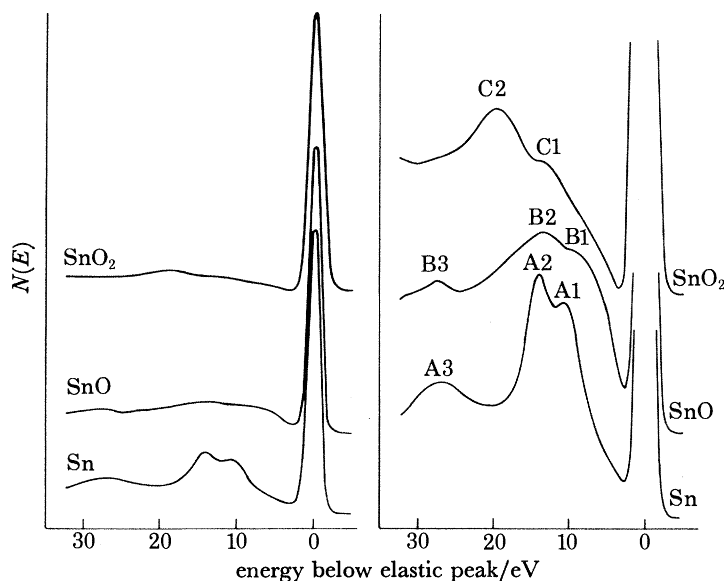

FIGURE 6. Demonstration by Powell (1979) of the possibility of using electron-loss structure for chemical identification. The Auger spectra for the two tin oxides were almost identical, but their loss spectra were quite different when amplified as on the right, and different also from tin metal. The primary energy was 400 eV and the energy resolution 0.25 %.

Electron energy-loss spectroscopy (*e.e.l.s.*)

In the spectrum of secondary electrons produced by primary electron irradiation can be found a variety of features due to discrete losses in energy from the primary energy. The most prominent of these are the so-called plasmon-loss peaks: they arise from the interaction of an outgoing electron with the sea of electrons in the conduction band of the specimen, causing collective oscillations of characteristic frequency and therefore of characteristic energy. Since the back-scattered primary electrons form the most intense feature in the spectrum for low primary energies, the plasmon-loss peaks associated with them are also the most intense, although they can be found associated with any intense sharp peak such as an Auger peak. The plasmon losses can sometimes be used for diagnostic purposes, as shown in figure 6 from Powell (1979), who found that the tin and oxygen Auger spectra from Sn^{II} oxide and Sn^{IV} oxide were almost identical, whereas the plasmon-loss spectra were quite different, and different also from metallic tin.

Downloaded from rsta.royalsocietypublishing.org

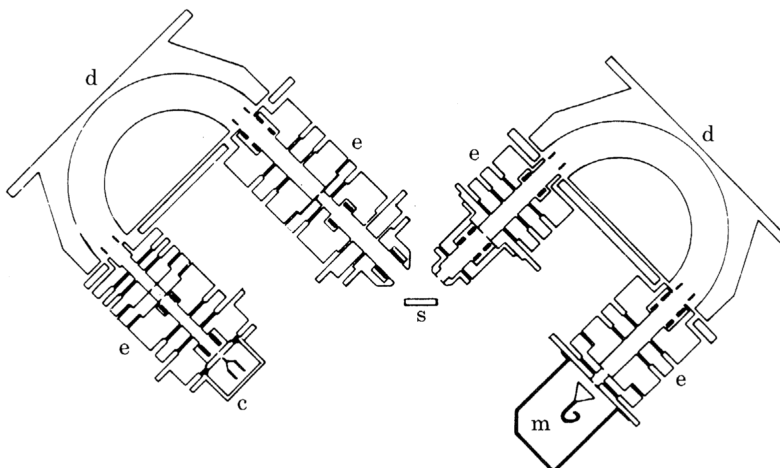

FIGURE 7. The spectrometer built by Backx *et al.* (1980) for low-energy electron-loss spectroscopy. The incident electron beam is generated on the left-hand side by a monochromator consisting of a 180° hemispherical dispersive deflector. An identical deflector analyses the energies of the backscattered electrons, at the right-hand side. The specimen is at s, c is the cathode, e the various electron optics, d the deflectors, and m the electron multiplier. Primary energies used are within the range 3–5 eV, primary currents about 5×10^{-10} A, and the typical energy resolution is about 8 meV.

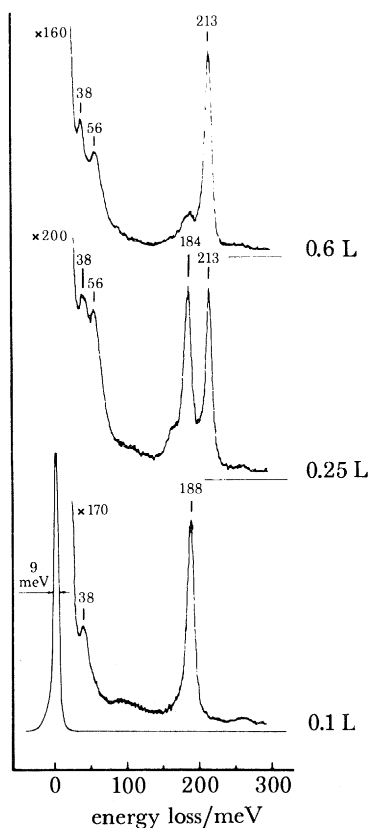

FIGURE 8. Electron energy-loss spectra of NO adsorbed on Pt(111) at 160 K, measured by Ibach & Lehwald (1978). Primary electron energy was 5 eV, and energy resolution 9 meV. The units of exposure are Langmuirs (1 L = 10^{-6} Torr s). See the text for a discussion of the various loss peaks identified in the spectra.

PHILOSOPHICAL TRANSACTIONS OF THE ROYAL SOCIETY A MATHEMATICAL, PHYSICAL & ENGINEERING SCIENCES

PHILOSOPHICAL TRANSACTIONS OF THE ROYAL SOCIETY A MATHEMATICAL, PHYSICAL & ENGINEERING SCIENCES

Downloaded from rsta.royalsocietypublishing.org

MATHEMATICAL, PHYSICAL & ENGINEERING SCIENCES
PHILOSOPHICAL TRANSACTIONS OF THE ROYAL SOCIETY A

The technique of e.e.l.s., however, has come to mean the observation and measurement of other kinds of discrete loss peaks. Polyatomic molecules undergo various forms of internal interatomic motion, particularly vibrational motion, and associated with each mode of vibration is again a characteristic frequency or energy. When molecules interact with surfaces, not only may their own inherent vibrational frequencies be altered, but additional vibrations may be introduced either between atoms in the molecule and atoms in the surface, or by the setting up of different modes in the molecule under the influence of the surface. Unlike the plasmon losses, which are normally 10–30 eV in magnitude, the vibrational losses are in the range 20–2000 meV. The experimental implications are that high-energy resolution is needed, so that the energy spread in the primary electron beam must be reduced to less than 10 meV, and the primary energy itself must be only a few electronvolts. To do this, hemispherical deflectors are used both on the input and output of the technique, one to select almost monochromatic electrons for the primary beam, and another to act as a high-resolution analyser. Such a system is shown diagrammatically in figure 7 and was constructed by Backx *et al.* (1980); its best resolution is claimed to be 8 meV. At such low energies and high resolution, extreme precautions have to be taken to avoid both interference with the electron paths by strong magnetic and electrostatic fields, and production of unwanted secondary electrons from any other surface except that of the specimen.

E.e.l.s. spectra taken by Ibach & Lehwald (1978) during the adsorption of NO on Pt are shown in figure 8. With increasing exposure to NO, the N–O stretching vibration of energy 188 meV (cf. 233 meV in the gas phase) decreases and almost disappears while a new loss peak at 213 meV appears, interpreted as being caused by interactions between adjacent absorbed NO molecules to form $(NO)_2$. The 38 meV loss is attributed to the Pt–N stretching vibration, which does not change with coverage since the NO molecule is adsorbed standing up on the surface with the nitrogen attached to the Pt. The additional loss observed at 56 meV at higher coverage is in agreement with the dimer model, since the selection rules predict three vibrational modes for $(NO)_2$.

Appearance potential spectroscopy (*a.p.s. or s.X.a.p.s.*)

As noted earlier, when a core hole is produced in an atom by electron irradiation, the ionized atom can relax either by the Auger process or by emission of a characteristic X-ray photon. For shallow core levels it was also noted that the latter process had a negligible probability compared with the Auger path; however, although negligible, the probability is not vanishing, and the X-ray photon emission can be used, as in the technique of soft X-ray appearance potential spectroscopy (s.X.a.p.s., or a.p.s. for short). In this technique the material is bombarded with low-energy electrons whose energy is varied continuously, typically from 0 to 1000 eV, and the total soft X-ray flux emitted is monitored as a function of the electron energy. The flux can be detected either directly by using a photon detector such as a barrier detector with a silicon surface cooled with liquid nitrogen (Andersson *et al.* 1974) or indirectly by measuring the photocurrent produced when the photons hit a photosensitive surface. The latter experimental arrangement is basically simple, and an example is shown in figure 9, from the work of Houston & Park (1971).

As the continuously increasing energy of the incident electrons passes through the threshold of ionization of a core level of an element present in the sample surface, the flux of emitted X-ray photons shows a sudden jump, or a step in the yield–energy plot. Such steps in the yield from chromium are shown in figure 10, from the same paper, at the thresholds for ionization of the

Downloaded from rsta.royalsocietypublishing.org

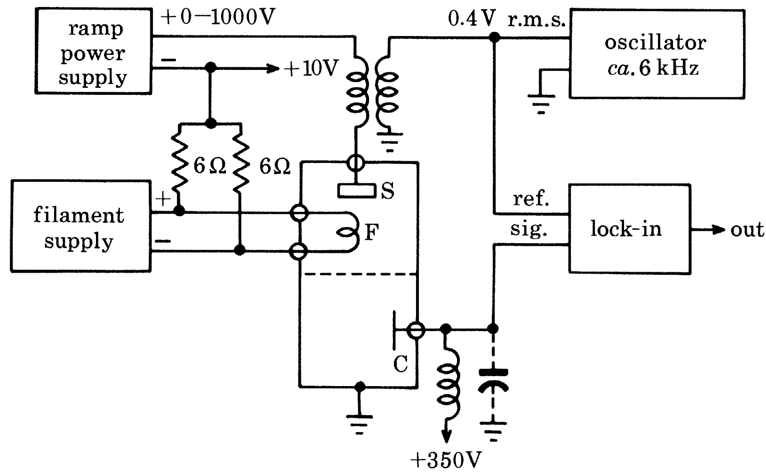

FIGURE 9. Experimental arrangement used by Houston & Park (1971) for a.p.s. measurements. Electrons from the source F strike the specimen S, and as their energy is ramped through thresholds for the production of soft X-rays from S, steps occur in the total X-ray yield. The X-rays generate photoelectrons from the internal surface of the vacuum container, which are collected by the collector C. The yield steps are enhanced by modulation of the ramp voltage, which provides differentiation of the total yield.

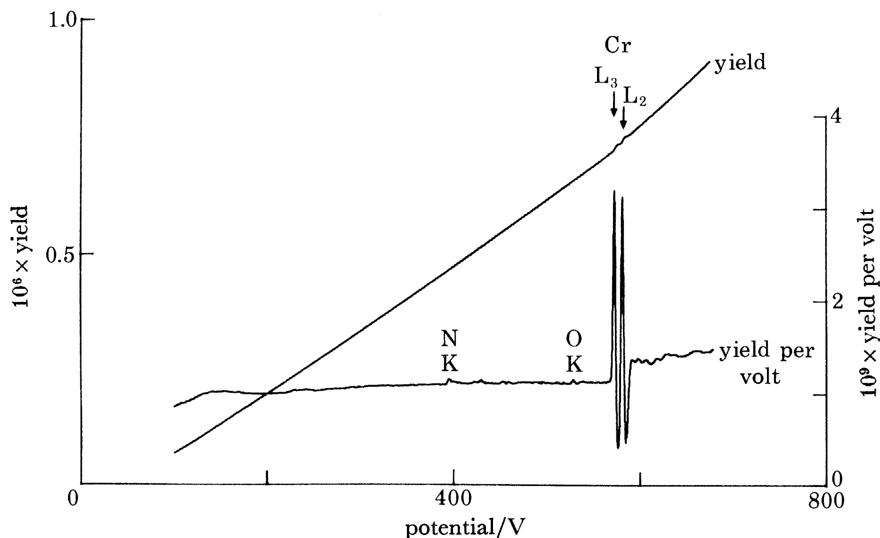

FIGURE 10. Comparison of the total soft X-ray yield with the differential yield, from chromium, as a function of the electron accelerating potential. As in A.e.s., the high background is effectively suppressed by differentiating the signal. The chromium L_3 and L_2 thresholds are very clear, and also visible are nitrogen and oxygen K thresholds from contamination on the surface. (From Houston & Park (1971).)

L_2 and L_3 core levels. Compared with the background flux the steps are small, and as in A.e.s. it is customary to differentiate the yield with respect to energy, as seen in the lower part of figure 10.

A threshold corresponds, of course, to the excitation of an electron from the core level to the first available empty electronic state, which will be situated just above the Fermi level. As the excitation energy is increased, transitions to other empty states become possible progressively, so that the yield function maps first the unfilled portion of the valence band and then other unfilled but allowed bands beyond the vacuum level. The technique therefore provides information not only about core level binding energies but also about the densities of unfilled states

Downloaded from rsta.royalsocietypublishing.org

above the Fermi level. The state density information is not easy to obtain directly, since a mathematical deconvolution of the data is necessary, but several workers have carried out the deconvolution successfully.

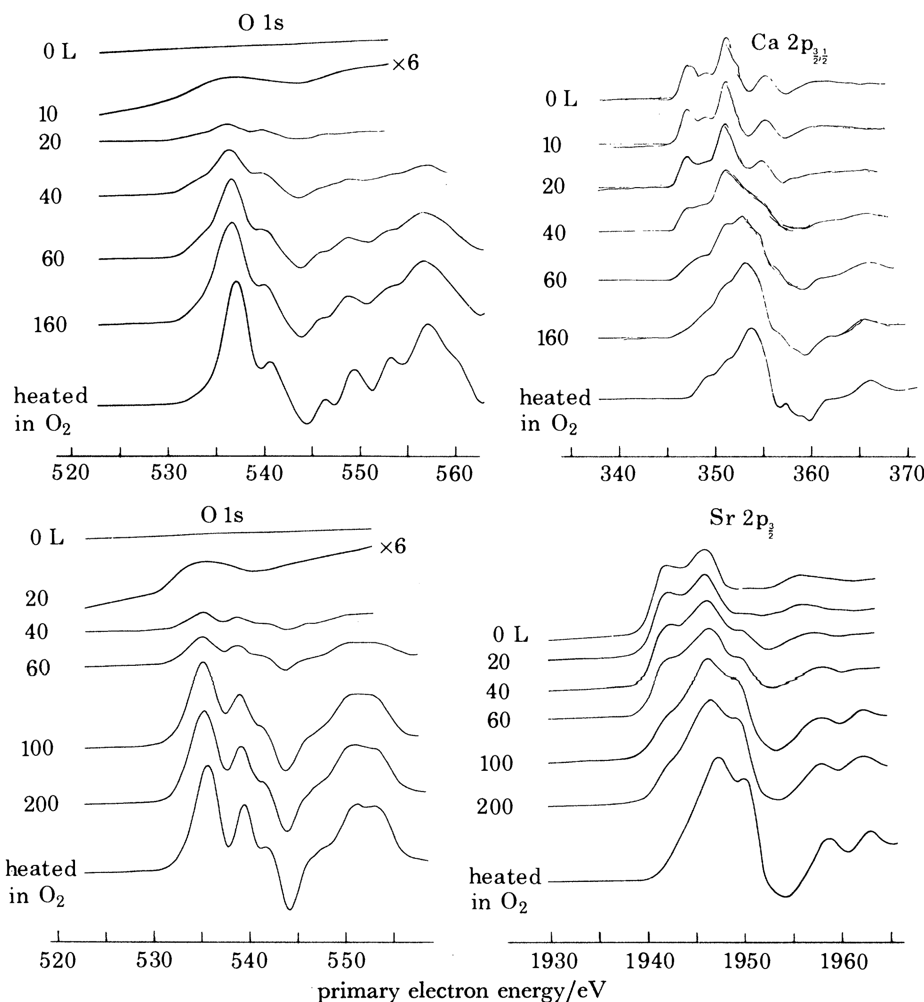

FIGURE 11. Changes in the oxygen, calcium and strontium a.p.s. spectra recorded by Nyberg (1977) during the oxidation of calcium and strontium films. The units of exposure are Langmuirs. In the low exposure region the oxygen peak is broad and featureless and the metal spectra unchanged. Above an exposure of *ca.* 50 L the oxygen spectra become full of fine structure, while at the same time the metal spectra alter drastically and shift towards spectra characteristic of the oxides.

An example of the application of a.p.s. is given in figure 11, from the work of Nyberg (1977). The O 1s, Ca 2p, and Sr 2p a.p.s. spectra are shown for increasing exposure of calcium and strontium films to oxygen, followed by heating in oxygen. At the lowest exposures the oxygen peak is merely broad and featureless, and there is no change in either of the metal spectra; the broad peak is attributed to the overlap of metal and oxygen valence orbitals without affecting the unfilled band structure of the metal. As the oxygen exposure increases, the oxygen spectrum becomes complex and the metal spectra are both shifted and altered. The final line shapes reflect differences in the unfilled densities of states between the metal and the oxide, while at

Downloaded from rsta.royalsocietypublishing.org

intermediate exposures, where the oxide is still not thick, the spectra are composites of incipient oxide and underlying metal spectra. The shifts in threshold correspond to the chemical shifts observable in other techniques, particularly in X-ray photoelectron spectroscopy (q.v.).

Electron-induced luminescence (e.i.l.)

The phenomenon of cathodoluminescence, i.e. luminescence caused by electron bombardment, has been known for many years, but has only recently been used as a technique for the study of surfaces. Many elements form cathodoluminescent oxides, so it should in principle be possible to follow the course of oxidation on those elements, or their alloys, and perhaps also derive information that could not be derived by any other technique. A demonstration of the possibilities has been made by Bastasz *et al.* (1978) in studying the oxidation of thorium.

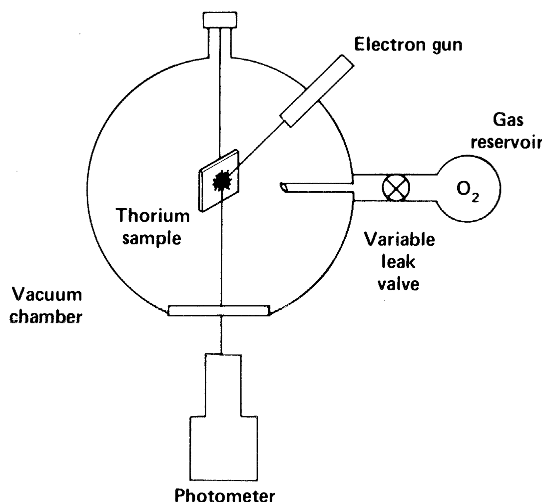

FIGURE 12. Experimental arrangement used by Bastasz *et al.* (1978) for the observation of e.i.l. from thorium and its changes during oxidation. Electron irradiation conditions were 3 keV primary energy, 20 μA primary current into an area of diameter less than 1 mm.

The experimental arrangement used by them was quite simple and is shown in figure 12. The photometer used for light intensity measurement was fitted with a telescope so that only light originating from the area irradiated by the electron beam was accepted. The emission spectrum was scanned by inserting a monochromator between the telescope and the photomultiplier.

Even the so-called 'clean' thorium was found to have a visible luminescence, attributed by the authors to the presence of small amounts of carbon or to other minor bulk impurities that segregated to the surface under the influence of the electron beam, but when oxygen was admitted the luminescent intensity grew rapidly. This intensity reached and maintained a plateau as long as oxygen was present at a fixed pressure. If the oxygen was pumped away, the intensity decreased to a level higher than that from the 'clean' surface. The plateau level was found to depend on the pressure of the oxygen, but the intensity on removing the oxygen was constant beyond a certain exposure. The effect is shown in figure 13 for two oxygen pressures, 7 and 15 μPa (i.e. *ca.* 5×10^{-8} and *ca.* 1×10^{-7} Torr, respectively).

The most interesting observation was made by combining A.e.s. analyses of the surface with the e.i.l. measurements. In the experiment shown in figure 14 elemental analyses were made at each of the labelled points during oxygen admission and subsequent removal. It was found that

PHILOSOPHICAL TRANSACTIONS OF THE ROYAL SOCIETY A MATHEMATICAL, PHYSICAL & ENGINEERING SCIENCES

PHILOSOPHICAL TRANSACTIONS OF THE ROYAL SOCIETY A MATHEMATICAL, PHYSICAL & ENGINEERING SCIENCES

Downloaded from rsta.royalsocietypublishing.org

although the surface oxygen concentration, as measured by A.e.s., altered by only 3 % between points C and E, the luminescent intensity dropped by 60 %. In other words, the oxygen in molecular form at the surface during exposure was enhancing the luminescent intensity out of all proportion to its concentration (if it is assumed that the probabilities of Auger emission from molecular and atomic oxygen at the surface are the same). Since the luminescent emission spectrum contained no fine structure characteristic of oxygen itself, but was a broad band peaking at 470 nm, similar to the photoluminescent spectra of thoria, the deduction is that the thorium substrate is interacting strongly with both dissociated and molecular oxygen in the luminescent process. This is perhaps the first indication of such an interaction with physically adsorbed molecular oxygen, and it could not have been identified by any other surface technique.

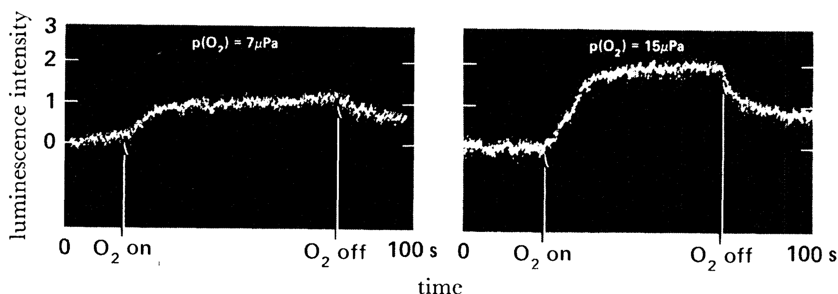

FIGURE 13. Variation in the e.i.l. intensity from a thorium specimen during exposure to oxygen. The intensity increased with oxygen admission until a plateau was reached; it remained there as long as the oxygen was present, and then decreased, but not to the original level, on removal of the oxygen. The level of the plateau reached during exposure was doubled when the partial pressure of oxygen was doubled. (From Bastasz *et al.* (1978).)

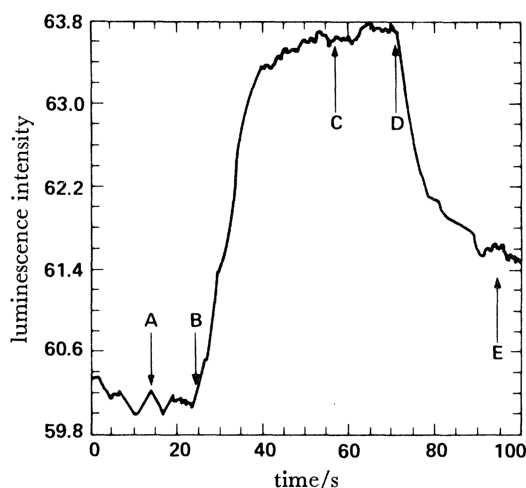

FIGURE 14. Variation in the e.i.l. intensity from thorium during exposure to oxygen. A.e.s. analyses were carried out at the labelled points. Oxygen was admitted at B and pumped out at D. The oxygen concentration at E was only slightly less than at C, indicating that the change in luminescent intensity was due to a very small fraction of the adsorbed oxygen, probably a weakly adsorbed molecular species. (From Bastasz *et al.* (1978).)

Electron-stimulated desorption (e.s.d.)

The interaction of an incident electron beam with adsorbed gases or other reactants on a surface can lead to major changes both in the elemental composition and in the rate of any reaction that is occurring. In general, such interference by the beam is highly undesirable, and

PHILOSOPHICAL TRANSACTIONS OF THE ROYAL SOCIETY A MATHEMATICAL, PHYSICAL & ENGINEERING SCIENCES

PHILOSOPHICAL TRANSACTIONS OF THE ROYAL SOCIETY A MATHEMATICAL, PHYSICAL & ENGINEERING SCIENCES

Downloaded from rsta.royalsocietypublishing.org

if an electron beam technique has unavoidably to be used in the study of a surface reaction, precautions have to be taken to minimize the effect, e.g. by defocusing the beam to reduce current density. On the other hand, the interaction can in some cases be put to use, rather than being dismissed as only a nuisance, and the usefulness arises when the beam–surface interaction leads to the desorption of ions, whose mass and energy can then be analysed. This is the technique of electron-stimulated desorption (e.s.d.); a variation of it that includes angular dependence of the emitted ions is called electron-stimulated desorption ion angular distribution

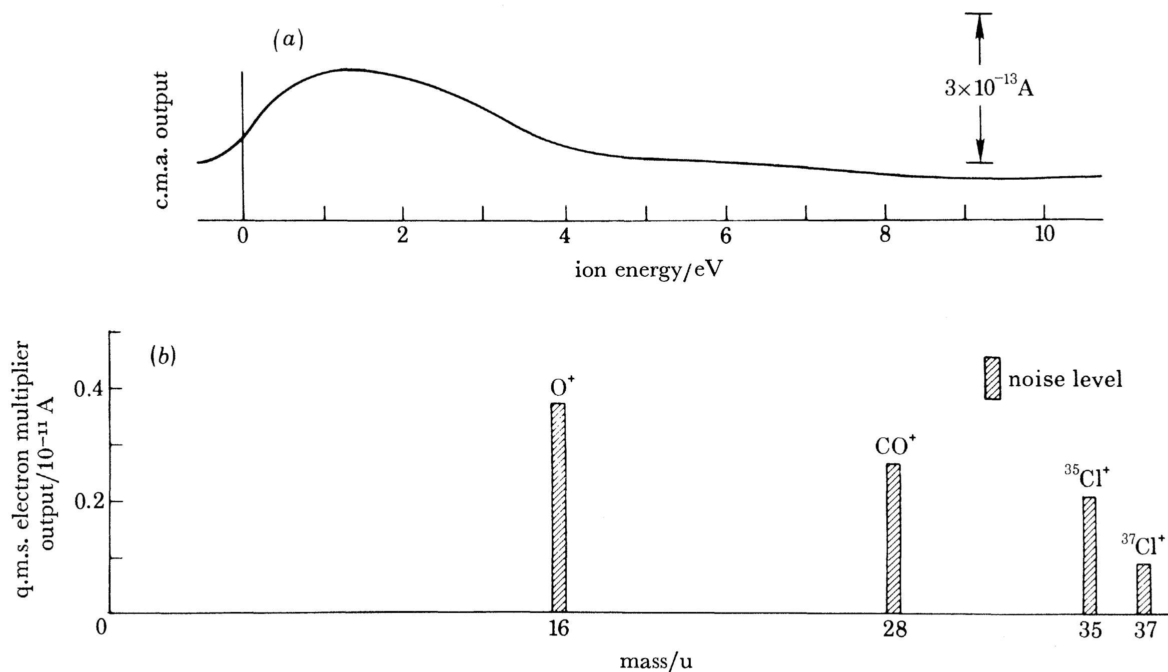

FIGURE 15. E.s.d. spectra obtained from a silicon (111) surface after adsorption of CO in the presence of a hot filament. Incident electron beam conditions were 100 eV, 2 μA. (*a*) The ion energy distribution as measured with a c.m.a.; (*b*) the mass spectrum as measured with a quadrupole mass spectrometer. When no hot filaments were present, no desorbed ion species were observed. From the data a cross section for electron-stimulated ionic desorption of 10^{-21} cm^2 at 100 eV was calculated. (From Dylla *et al.* (1978).)

(e.s.d.i.a.d.). For e.s.d. primary electron energies of 300–1000 eV and primary current densities of 0.1–1.0 μA cm^{-2} are used, and the desorbed ions are analysed either for mass in a quadrupole mass spectrometer, or for energy in the type of energy analyser, the cylindrical mirror analyser, normally used in A.e.s. In fact, all e.s.d. experiments are carried out in conjunction with complementary A.e.s. measurements.

A combined mass and energy analysis for desorption from an adsorbed layer of CO on silicon is shown in figure 15, from the work of Dylla *et al.* (1978). The mass spectrum shows some small peaks due to O^+ and CO^+ (as well as some chlorine impurity peaks); the adsorption of CO in that case was carried out in the presence of a hot filament (i.e. from ion gauges, from the mass spectrometer or from the electron gun). When no filaments in the system were hot, no desorption peaks could be found, indicating prior dissociation of the CO by the hot filaments into fragments of higher reactivity. In the energy spectrum two broad peaks can be seen, one at *ca.* 1.5 eV and another at *ca.* 6 eV. These two peaks can be seen more clearly in the adsorption of oxygen rather than CO, for example on molybdenum as studied by Bauer & Poppa (1979).

Downloaded from rsta.royalsocietypublishing.org

Figure 16 shows that the 1.5 eV peak is characteristic of the early stages of reaction and the 6 eV peak of the later stages, in fact of the formation of incipient oxide. The additional peak at 2.6 eV evident in figure 16 was shown, interestingly, to be an electron irradiation artefact and not characteristic of the oxidation mechanism.

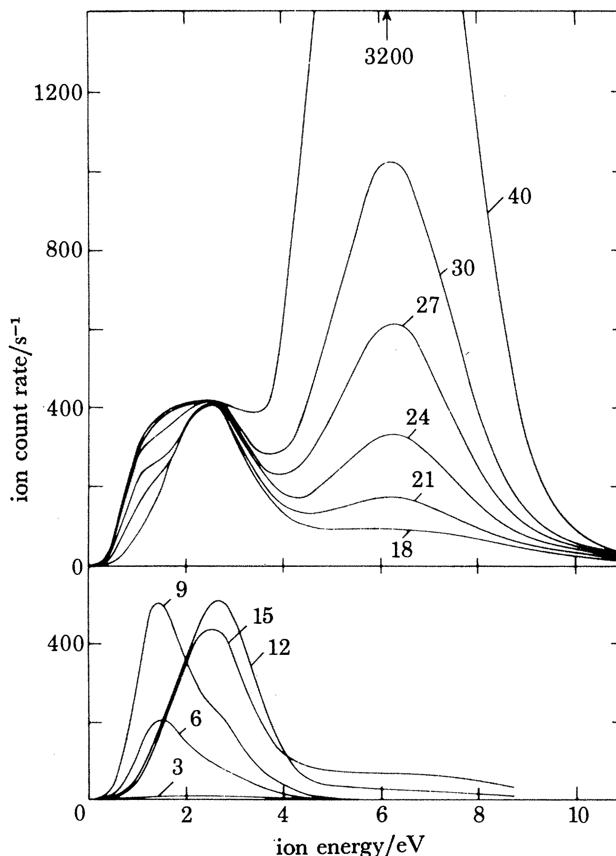

FIGURE 16. Dependence of the energy distribution of the oxygen ion desorbed by electron stimulation from a molybdenum (100) surface, on the time of exposure to 2×10^{-9} Torr of oxygen at 300 K; the labels on the curves indicate exposure times in minutes. Incident electron beam conditions were 300 eV, 0.4 μA. The peak at 1.5 eV is characteristic of the early stages of oxidation and the 6 eV peak of the later stages, but that at 2.6 eV is an electron irradiation artefact and not part of the oxidation process. Background pressure was 5×10^{-11} Torr. (From Bauer & Poppa (1979).)

PHOTON EXCITATION

X-ray photoelectron spectroscopy (*X.p.s.*)

This is possibly the most widely used of current surface analytical techniques, and in principle it is very simple. The specimen is irradiated with X-ray photons of low energy, typically Al K_α (1486.6 eV) or Mg K_α (1253.6 eV), when photoionization of core levels in atoms near the surface occurs.

Interaction of an X-ray photon of energy $h\nu$ with an electron in a core level of binding energy E_b leads to ejection of a photoelectron with kinetic energy given by the relation

$$E_{kin} = h\nu - E_b. \tag{1}$$

Since electron energies have to be measured in an energy analyser, i.e. accepted by a collecting surface at some stage, then a small work function term should be added to (1); however, it

Downloaded from rsta.royalsocietypublishing.org

remains effectively constant. Equation (1) shows that there is a direct relation between the measured kinetic energy of the photoelectron and the binding energy of the level from which it came, since the photon energy is kept constant, and thus the technique is a spectroscopic one, no two elements having the same set of electronic binding energies. For the same reason, any changes in the binding energy of a level consequent upon changes in the chemical surroundings or state of combination of the atom to which it belongs are reflected immediately in a shift in the photoelectron peak. This is the so-called 'chemical shift'.

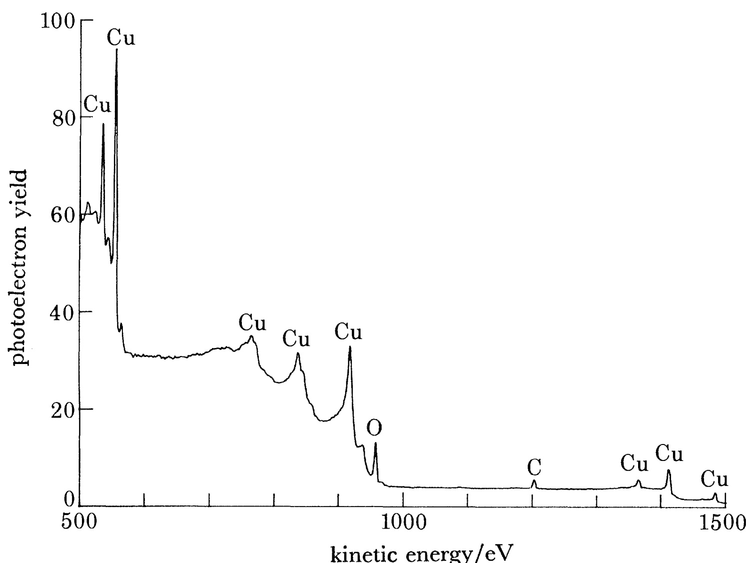

FIGURE 17. Wide-scan X-ray photoelectron spectrum from a slightly contaminated copper surface, with Al K_{α} radiation (1486.6 eV, power 400 W, pass energy 100 eV) as the primary source. The most intense copper peaks are due to photoelectrons ejected from the 2p levels, appearing to the left between 500 and 600 eV, while between 1350 and 1500 eV there are, in order, the 3s, 3p and 3d photoelectron peaks. Also visible are the X-ray excited copper LMM Auger peaks between 750 and 920 eV. Small photoelectron peaks from oxygen and carbon contamination on the surface can also be seen.

Since the ionized atom can of course relax by the ejection of an Auger electron, just as described for A.e.s., features due to both photoelectrons and Auger electrons appear in the spectrum. When the interest is almost entirely centred on the photoelectron peaks, the technique is called X-ray photoelectron spectroscopy (X.p.s., but often called e.s.c.a.), but when it is the Auger peaks that are being studied then it is called X-ray excited Auger electron spectroscopy (X.A.e.s.), to be discussed below.

An example of an X-ray excited spectrum containing both photoelectron and Auger peaks is given for copper in figure 17. Note the appearance in the energy range of the figure of photoelectron peaks from the 2p, 3s, 3p and 3d levels of copper, and of Auger peaks due to the copper LMM transitions. The latter are in fact in the same sequence as the LMM spectra for some other transition metals already shown in figure 2, only in this technique the spectrum does not need differentiation. Also seen in the copper spectrum are some small peaks due to residual contamination by oxygen and carbon.

Chemical shifts can vary from a few tenths of an electronvolt to several electronvolts, and a striking example is shown in figure 18. There the tungsten 4f photoelectron peaks have been recorded, firstly in the atomically clean condition in the upper curves, and then after slight oxidation to produce a very thin oxide film. The film is thin enough for photoelectrons from the

Downloaded from rsta.royalsocietypublishing.org

underlying metal to penetrate to the vacuum, and the result is a composite spectrum in which both metallic and chemically shifted tungsten 4f peaks appear together. In this case the chemical shift is large enough to move the 'oxide' 4f doublet completely clear of the 'metal' doublet, giving rise to four peaks well resolved from each other. In most cases, however, the shift is smaller and overlapping of peaks results, with the consequent need for peak stripping and curve synthesis procedures.

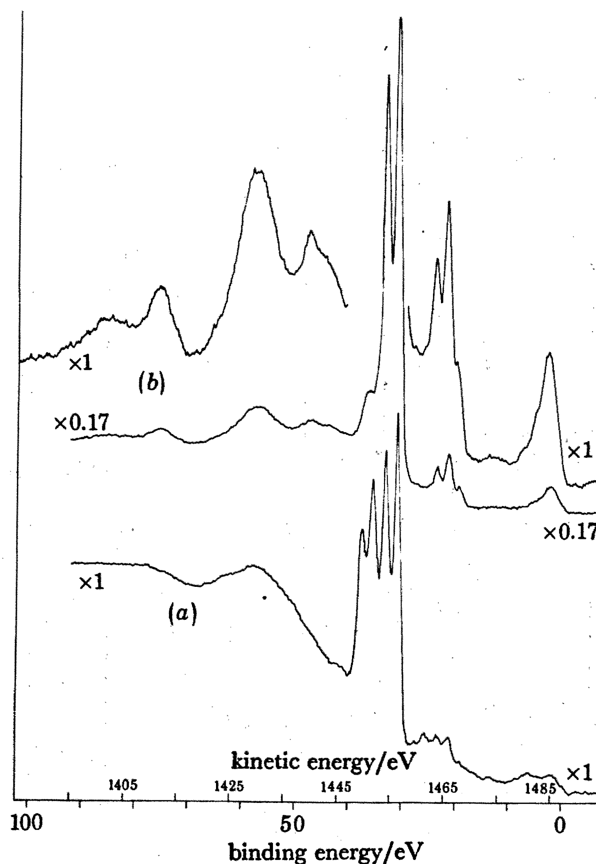

FIGURE 18. X-ray photoelectron spectrum of tungsten (Al K_α radiation (1486.6 eV)) in an atomically clean condition (curves *b*), and after slight oxidation to produce a very thin oxide film (curve *a*). The film is sufficiently thin to allow photoelectrons from the underlying metal to penetrate to the vacuum without being scattered. The result is a composite spectrum of the chemically shifted 4f peaks and the metallic 4f peaks, the shift in this case being large enough to give rise to four peaks well separated from each other.

The other type of information provided by X.p.s. concerns the electrons of lowest binding energy, i.e. those in the valence band of a solid. Since they are of course those photoelectrons of highest *kinetic* energy, according to (1), they will not be quite as specific to the outer surface itself as those at lower energy, and valence band spectra recorded by X.p.s. are generally regarded as more characteristic of the bulk than those recorded, say, by ultraviolet photoelectron spectroscopy (see below). In figure 17 the 3d photoelectrons from copper form of course the valence band spectrum, but on the scale of the figure it is impossible to see any detail. Figure 19, from Hedman *et al.* (1971), gives examples of detailed valence band spectra for various metals and their alloys. Some marked differences can be seen between the spectra of different metals, and the figure shows also that in the particular alloys chosen, the alloy spectrum is simply a

MATHEMATICAL, PHYSICAL & ENGINEERING SCIENCES
THE ROYAL SOCIETY A
PHILOSOPHICAL TRANSACTIONS OF

MATHEMATICAL, PHYSICAL & ENGINEERING SCIENCES
THE ROYAL SOCIETY A
PHILOSOPHICAL TRANSACTIONS OF

Downloaded from rsta.royalsocietypublishing.org

composite of the spectra of the individual elements in the alloying proportions. For other alloys or intermetallics, the valence band spectra would not necessarily resemble those of the constituents.

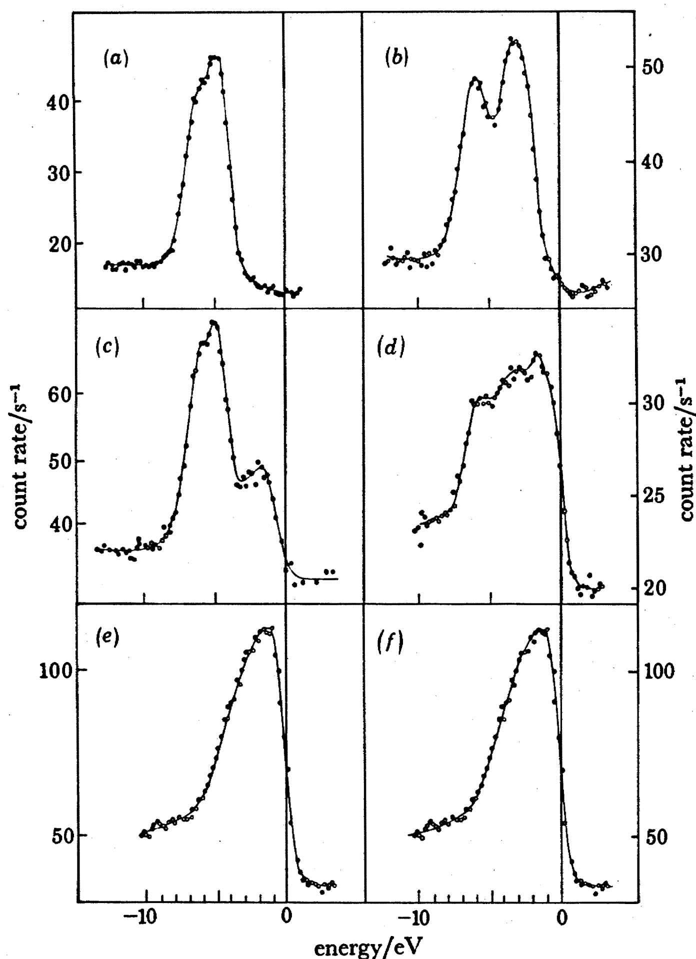

FIGURE 19. X-ray excited spectra of the valence bands of (*a*) silver, (*b*) gold, (*e, f*) palladium and some alloys ((*c*) $Ag_{0.71}Pd_{0.29}$, (*d*) $Au_{0.45}Pd_{0.55}$) recorded by Hedman *et al.* (1971). The energy scale is that of binding energy, with the zero of energy taken as the Fermi level of the metal. The spectra of the alloy valence bands are composites of the constituent valence bands in proportion to the alloy composition.

X-ray excited Auger electron spectroscopy (*X.A.e.s.*)

As described above, this technique really only amounts to using different features, the Auger peaks, in the electron emission spectrum recorded in X.p.s., which uses principally the photoelectron peaks. The advantages of X.A.e.s. over conventional A.e.s. are that higher-energy resolution is obtainable, spectral recording is in the direct rather than in the differential mode, and that disturbance from an incident electron beam is absent. On the other hand, recording times are longer and there is the possibility of interference from photoelectron peaks. In general, X.A.e.s. has therefore been restricted in application to studies either of the fine structure associated with certain Auger peaks of certain elements, or of surface reactions where any possibility of electron beam effects must be eliminated. One expanding application is in measurement of the so-called 'Auger parameter', first devised by Wagner (1978). This quantity sets out to

PHILOSOPHICAL TRANSACTIONS OF THE ROYAL SOCIETY A MATHEMATICAL, PHYSICAL & ENGINEERING SCIENCES

PHILOSOPHICAL TRANSACTIONS OF THE ROYAL SOCIETY A MATHEMATICAL, PHYSICAL & ENGINEERING SCIENCES

Downloaded from rsta.royalsocietypublishing.org

provide a more sensitive measure of the chemical state of an element than just the positions of its photoelectron peaks, by combining Auger and photoelectron peak positions measured in the same spectrum. It is equal to the sum of a chosen Auger peak kinetic energy and a chosen photoelectron peak binding energy, less the kinetic energy of the exciting photons, and is proving to be a useful 'fingerprint'.

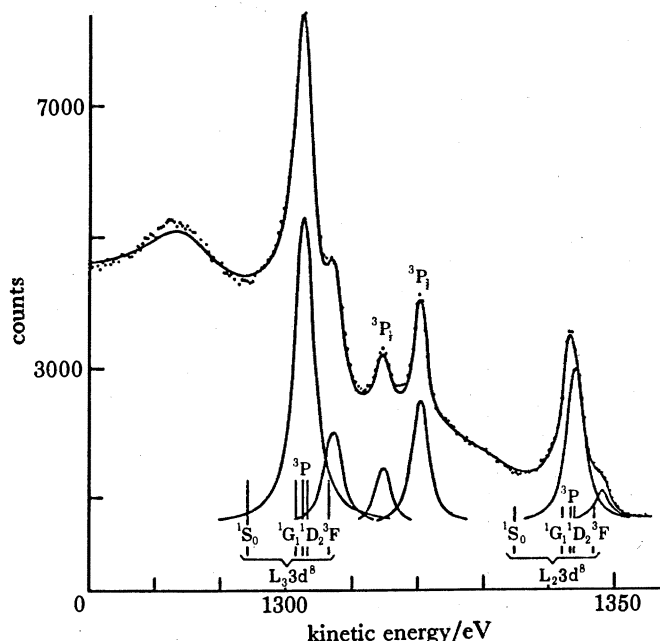

FIGURE 20. The X-ray excited $L_{2,3}M_{4,5}M_{4,5}$ Auger spectra of selenium measured by Weightman *et al.* (1975). The points are the experimental measurements, and the full line a computer fit to the spectrum by using the individual final-state term energetic positions and intensities shown at the bottom, broadened to take account of instrumental broadening. An inelastic background has also been added to the computed spectrum. Also visible are the two selenium 3p photoelectron peaks.

Figure 20 shows an example of a high-resolution Auger spectrum recorded in the direct mode, the $L_2M_{4,5}M_{4,5}$ and $L_3M_{4,5}M_{4,5}$ peaks of selenium, from the work of Weightman *et al.* (1975). The points are the experimental measurements and the full line a fit by computer with the use of the individual final state energetic positions shown by vertical lines, broadened to take account of instrumental broadening, and weighted, together with a calculated inelastic background. The selenium 3p photoelectron peaks also appear in the spectrum.

Synchrotron radiation photoelectron spectroscopy (*s.r.p.s.*)

As its name suggests, this technique is really only a variation of X.p.s., but it merits designation as a separate technique because it uses not a source of fixed line energy but a source whose photon energy can be varied. In a synchrotron the circulating electrons are accelerated to relativistic speeds, and under those conditions emit soft X-radiation tangentially to their orbits as they are constrained to their circular paths. According to the diameter of the orbit and to the energy to which they are accelerated, the emitted X-ray energy spectrum peaks in intensity at different energies. However, the peak is not sharp, and there is considerable and usable intensity over a wide range of photon energies. Energy selection is performed by a variety of different types of monochromator. A typical range covered would be from 40 to 200 eV.

Downloaded from rsta.royalsocietypublishing.org

Variation of the incident photon energy can have two effects on the photoelectron spectrum not easily separable. Firstly, there is an escape depth effect: reference to figure 1 shows that between 40 and 200 eV the average escape depth passes through a minimum, although not a particularly pronounced minimum; the variation is probably less than twofold. Secondly, there is an energy-dependent photoemission cross section effect. This can be quite dramatic: for

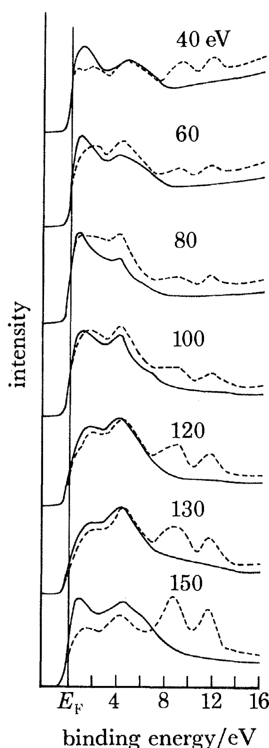

FIGURE 21. Synchrotron radiation excited photoemission spectra of platinum (111) before (——) and after (-----) adsorption of 5 L of CO, as a function of primary photon energy in the range 40–150 eV. The twin features visible are due to the 4σ (at *ca.* 11.8 eV) and the (5σ + 1π) (at *ca.* 8.7 eV) molecular orbitals of CO, and their intensities relative to the platinum valence band vary by about fourfold between 80 and 150 eV. The energy resolution used was 0.8 eV. (Redrawn from Apai *et al.* (1976).)

example, Apai *et al.* (1976) have shown that the integrated intensity of the platinum valence band decreases by a factor of 50 over the photon energy range 40–150 eV, related to the energy dependence of the 5d ionization cross section. This variation was put to use by Apai *et al.* in a study of the adsorption of CO on platinum. The s.r.p.s. spectra obtained for the clean and CO-covered platinum surface at various photon energies are shown in figure 21. All the Pt + CO spectra show two features, P_1 at about 11.8 eV and P_2 at about 8.7 eV, attributable to the 4σ and the (5σ + 1π) CO molecular orbitals, respectively, but their intensities relative to the substrate valence band vary by at least fourfold, from about 80 to 150 eV. This variation is given in figure 22. Most of the enhancement of the adsorbate intensity is due to the above-mentioned steep decrease in the platinum 5d cross section.

It is possible, then, to choose a photon energy in s.r.p.s. that will selectively enhance one or more features in the spectrum, relative to others, especially to the substrate spectrum, and thus increase the sensitivity with which adsorbate interaction can be observed. Alternatively, if it is desired to study the effect of surface reaction on the electronic structure of the substrate itself, it should be possible to find another available photon energy at which the features are

Downloaded from rsta.royalsocietypublishing.org

minimized relative to those of the substrate. Further selectivity can be introduced by the angular dependence of the photoemission, and in addition such studies can yield information on bonding symmetry, especially when the 100 % plane polarization of the synchrotron radiation is employed.

Ultraviolet photoelectron spectroscopy (u.p.s.)

In operation and principle this has many similarities to X.p.s., in that the energies of photoelectrons are analysed, and in fact the same energy analyser is used for both. As the name suggests, the main difference lies in the source of photons that is used, an ultraviolet lamp rather than an X-ray tube. In a typical u.v. source, photons are produced in a capillary discharge, the

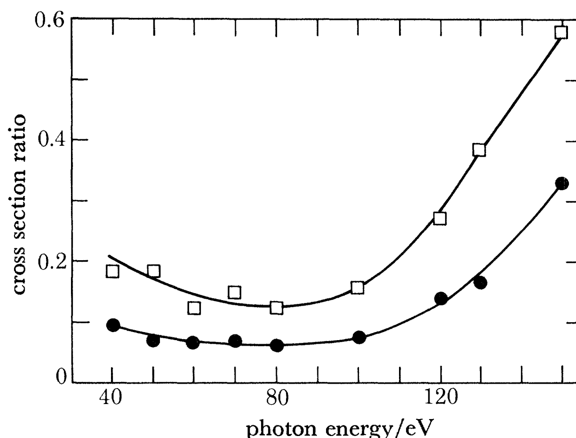

FIGURE 22. Variation in intensity of the two peaks due to CO adsorption shown in figure 21, with respect to the integrated intensity of the platinum valence band. □, σ (P_2/σ(Pt 5d); ●, $\sigma(P_1)/\sigma$(Pt 5d). P_1 is the 4σ peak and P_2 the $(5\sigma+1\pi)$ peak. The variation is caused principally by a steep decrease in 5d ionization cross section with increasing photon energy in the energy range chosen. (Redrawn from Apai *et al.* (1976).)

photon energy required being decided by the nature of the noble gas used in the discharge, and its pressure. It is straightforward, for example to produce monochromatic photons by excitation of the He I (21.21 eV), He II (40.8 eV), Ne I (16.8 eV), Ne II (26.9 eV) and Ar I (11.8 eV) lines. Photoelectrons excited by any of these sources clearly can be ejected only from the shallowest electronic levels in the solid, i.e. from the valence band, and the technique is indeed a valence band spectroscopy. At such low kinetic energies it is necessary, if adequate energy resolution is to be maintained, to work at much lower analyser energies (pass energies) than is normal in X.p.s., which is really the only other difference in operation between the two techniques.

U.p.s. has been used very extensively to study valence band structure in its own right, i.e. from pure metals and alloys whose surfaces have been cleaned, and also to study the drastic changes that take place in the structure when reactions or other treatments occur at the surface. In its angle-resolved variation, called a.r.u.p.s., the variations in the valence band structure with direction of ejection of the photoelectrons, or in other words, with direction in the crystal, have been used for correlation with theoretical band structure calculations.

In figure 23, from Eastman (1971), is shown the valence band spectrum of titanium taken at a variety of photon energies. Just below the zero of energy, at the Fermi level, can be seen the peak due to the d-band of the metal, with a fine structure that changes in relative magnitude with photon energy. These changes arise, among others, from variations in the relative photoionization cross section of individual components in the band; the data of figure 23 were

PHILOSOPHICAL TRANSACTIONS OF THE ROYAL SOCIETY A MATHEMATICAL, PHYSICAL & ENGINEERING SCIENCES

PHILOSOPHICAL TRANSACTIONS OF THE ROYAL SOCIETY A MATHEMATICAL, PHYSICAL & ENGINEERING SCIENCES

Downloaded from rsta.royalsocietypublishing.org

recorded, of course, at a particular angle of acceptance of photoelectrons from the surface, and an a.r.u.p.s. experiment would provide even more information about the variation in cross section in different crystal directions.

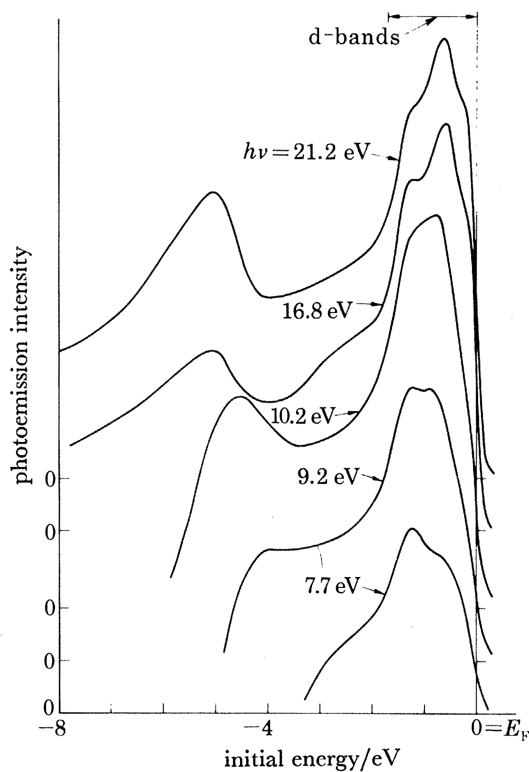

FIGURE 23

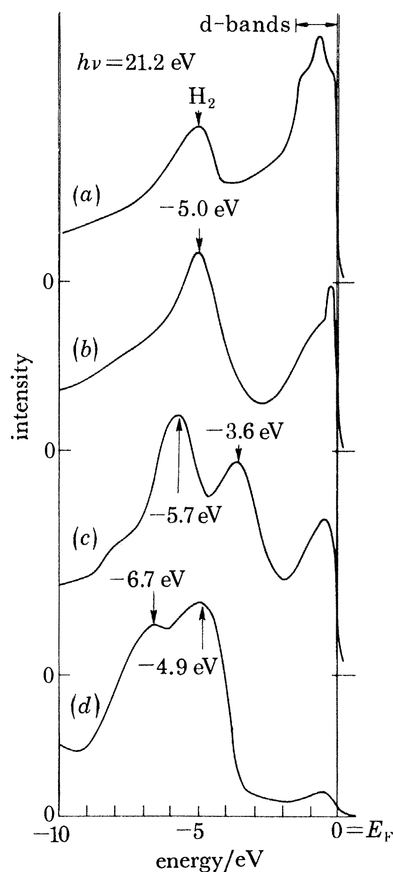

FIGURE 24

FIGURE 23. The valence band spectrum of titanium excited by several ultraviolet line sources. Between 0 eV, at the Fermi level, and about 2 eV is the d-band structure of the metal; the relative contributions to the d-band from its component bands change with energy due to changing cross sections. The peak at *ca.* 5 eV seen in the upper two spectra is anomalous in comparison with neighbouring transition metals, and its origin is demonstrated in figure 24. (From Eastman (1971).)

FIGURE 24. Valence band spectra of titanium excited by He I radiation, after reaction with (*b*) H_2, (*c*) CO and (*d*) O_2, compared with the 'clean spectrum' (*a*). Additional characteristic structures appear below the d-band, which is itself attenuated. The structure due to H_2 adsorption is identical with that seen in the 'clean' spectrum, indicating that the anomalous structure seen in the latter is due to the residual hydrogen in the vacuum system. (From Eastman (1971).)

Also seen in figure 23 at about 5.0 eV below the Fermi level, in the upper spectra, is a peak that seems anomalous when comparison is made with the u.p.s. spectra of neighbouring transition metals. Figure 24 gives a clue to the reason. There the u.p.s. spectra for 21.2 eV excitation recorded after the reaction of titanium with various gases are compared. In all cases the d-band peak is reduced, particularly after reaction with oxygen: in addition there are structures induced several electronvolts below the Fermi level, characteristic of each adsorbate. The interesting observation is that the reaction with hydrogen produces structure in a position identical to that found with the 'clean' metal. The deduction is that even after thorough cleaning of a titanium surface, the metal reacts with, and absorbs, hydrogen so readily from the

PHILOSOPHICAL TRANSACTIONS OF THE ROYAL SOCIETY A MATHEMATICAL, PHYSICAL & ENGINEERING SCIENCES

PHILOSOPHICAL TRANSACTIONS OF THE ROYAL SOCIETY A MATHEMATICAL, PHYSICAL & ENGINEERING SCIENCES

Downloaded from rsta.royalsocietypublishing.org

ambient in the vacuum system that it would be difficult, if not impossible, to eliminate the additional structure in the u.p.s. spectrum.

The application of u.p.s. to the study of surface reactions has been very fruitful, especially when the technique is applied in combination with other techniques such as A.e.s. and X.p.s. to derive maximum information. An example of an application of this type is shown in figure 25

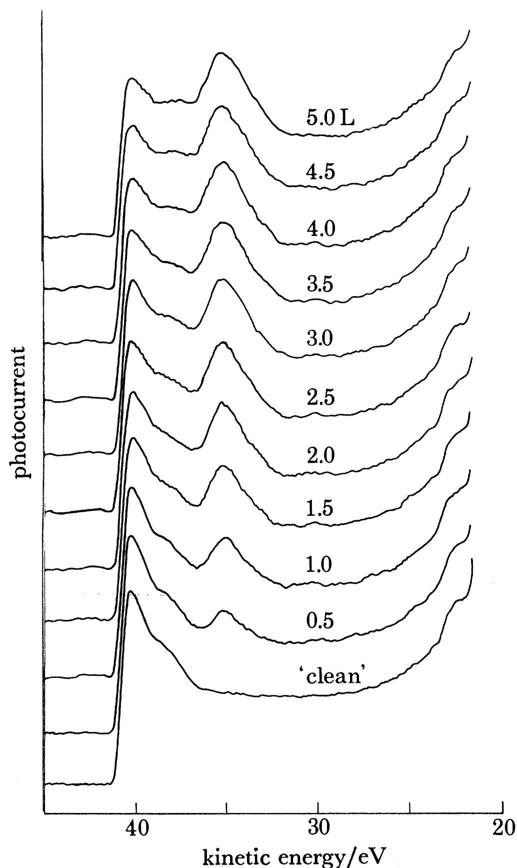

FIGURE 25

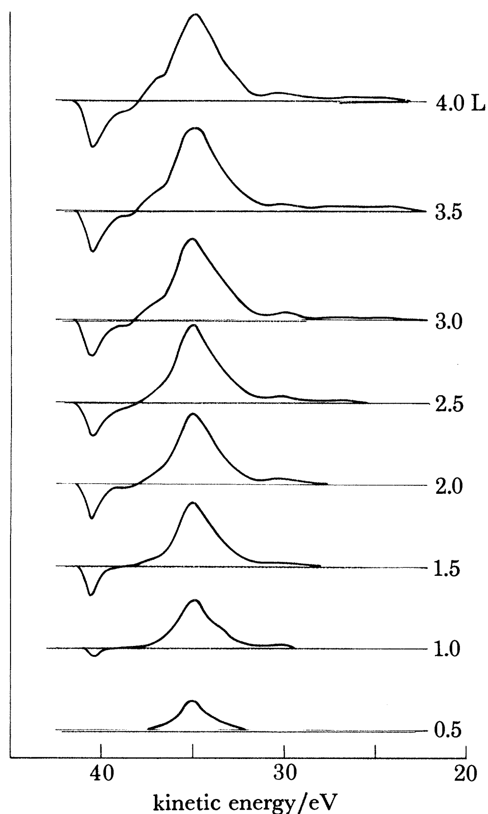

FIGURE 26

FIGURE 25. Photoelectron spectra excited by He II radiation, of energy 40.8 eV, from the surface of an iron (110) crystal during adsorption of oxygen at room temperature. The additional feature that appears and grows with exposure is due to electrons excited in the orbitals formed by formation of a surface 'molecule' between the dissociated oxygen and surface iron atoms.

FIGURE 26. The result of subtracting the clean iron He II u.p.s. spectrum at the bottom of figure 25 from the other spectra in that figure. The growth of the additional band due to adsorbed oxygen can be seen clearly, but also it can be seen that there is an increasing deficiency of electron charge in the iron d-band with increasing exposure.

in which the He II u.p.s. spectra from the (110) surface of an iron single crystal at room temperature have been recorded as a function of oxygen exposure (1 L = 10^{-6} Torr s), starting with the spectrum of the clean surface. In figure 26 the clean spectrum has been subtracted from all the others to provide difference spectra in which it can be seen clearly that two changes take place in a progressive manner. Additional structure due to the presence of dissociated oxygen at the surface in combination with iron appears and grows rapidly, while at the same time a deficiency of electron density in the iron d-band occurs, and also increases with exposure. Such

Downloaded from rsta.royalsocietypublishing.org

information, when taken in conjunction with information from other techniques, allows the construction of a mechanistic model for the course of the surface reaction.

Photoelectron spectromicroscopy (*p.e.s.m.*)

This is a very recent variation and extension of the technique of u.p.s., and, it is hoped, of X.p.s. also as a future development. It holds out promise of overcoming the major disadvantage of the photoelectron spectroscopies compared with A.e.s. and s.s.i.m.s. (*q.v.*), that of lack of spatial resolution.

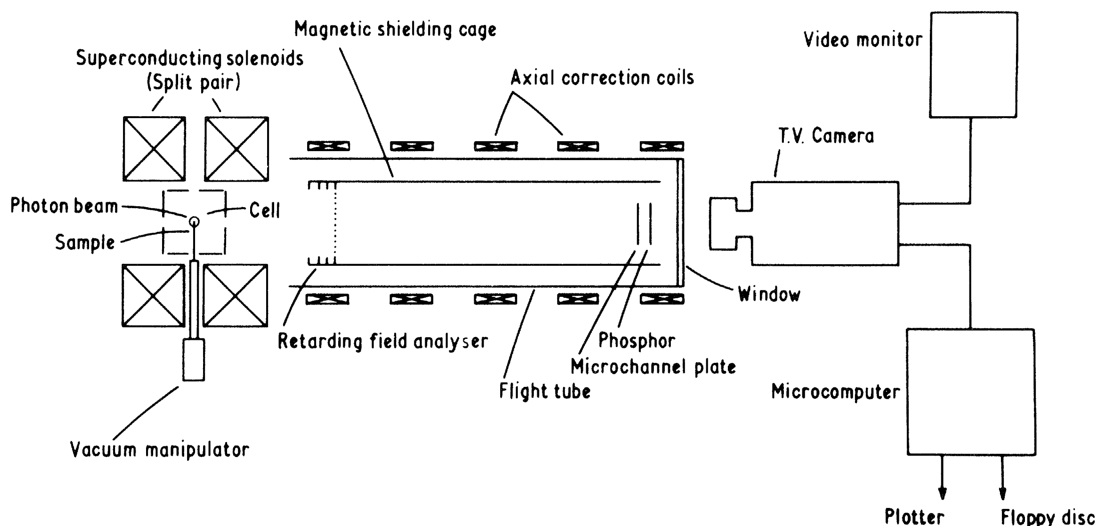

FIGURE 27. Prototype instrument built by Beamson *et al.* (1981) for p.e.s.m. Photoelectrons ejected from the sample by He I radiation are constrained to travel along the divergent field lines produced at the sample position by a very intense magnetic field of 7.7 T. In the flight tube a system of coils produces a progressively decreasing magnetic field that provides a magnification of the photoemitting area of the sample. The photoelectrons are detected on a microchannel plate and their image viewed on a phosphor screen. Lateral resolution in this instrument is of the order of 1 μm.

The new development is based, as described by its originators Beamson *et al.* (1981), on the capability of an axially symmetric divergent magnetic field of generating an enlarged image of a photoemitting surface while preserving the original energy distribution. In such a field the orbital momentum of an electron is conserved, as well as its total energy, so that any component of energy transverse to the magnetic flux lines is converted eventually to energy along the magnetic axis. Thus after a sufficiently large change of field, the original photoelectron energy, i.e. that possessed on leaving the surface, is concentrated almost entirely in the axial motion. Another important feature is that the helical trajectory of an electron adjusts itself along the diverging flux line so that orbital momentum is conserved, the orbital radius thus being proportional to the magnification. These features have the important practical consequences that an electron leaving the surface at a particular point is constrained closely to the flux line through that point, and that retarding potential energy analysis with the use of a planar field can be performed at any convenient image plane in the low-field region far removed from the surface.

Considerations of the lateral resolution to be expected show that for a field strength, at the specimen, of 8 T, the lateral resolution would be 10^3, 10^2 and 10 nm for electron energies of 500,

PHILOSOPHICAL TRANSACTIONS OF THE ROYAL SOCIETY A MATHEMATICAL, PHYSICAL & ENGINEERING SCIENCES
PHILOSOPHICAL TRANSACTIONS OF THE ROYAL SOCIETY A MATHEMATICAL, PHYSICAL & ENGINEERING SCIENCES

Downloaded from rsta.royalsocietypublishing.org

5, and 0.05 eV, respectively. The depth resolution depends, of course, on the average escape depth of the photoelectrons, as in the other secondary electron techniques, which in turn depends on the photoelectron kinetic energies according to figure 1.

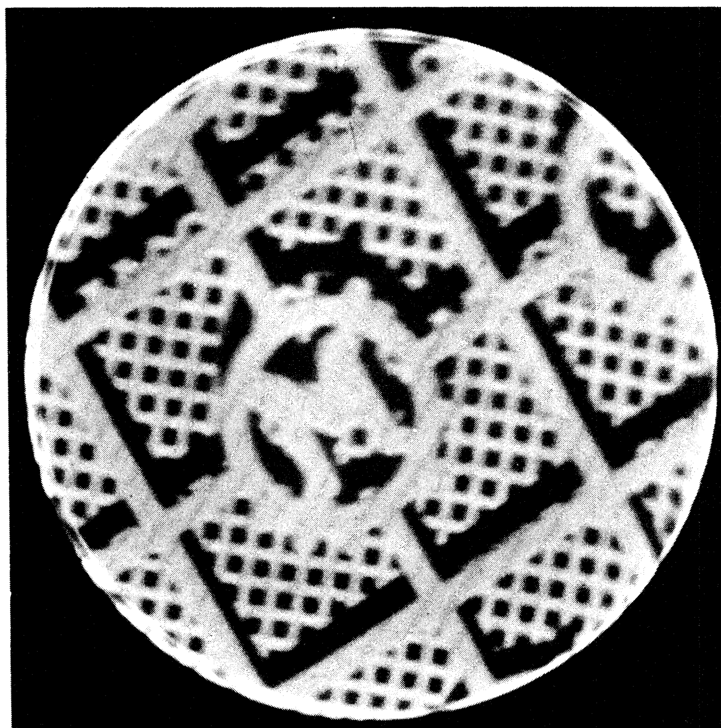

FIGURE 28. An example of the resolution obtained with the pre-production p.e.s.m. built by A. J. Dixon, K. A. Gehring & M. Keenlyside (personal communication 1982). The image is of two grids, a gold finder grid (with the letter M visible) on top of, but not in contact with, a 400 cm^{-1} mesh nickel grid. The spaces in the nickel mesh are about 18 μm, and the bars about 7 μm, in width. Shadows of the upper on the lower grid can be seen. The image was taken by He I photon illumination, and at a central magnetic field of 7.0 T. No energy selection was used, i.e. all photoelectrons were collected to form the image. (By courtesy of Thor Research Instruments, U.K.)

A prototype instrument built by Beamson *et al.* (1981) is shown in figure 27. The very high divergent magnetic field required is provided by a superconducting solenoid in a split-pair configuration, providing a maximum central field of 7.7 T. After leaving the solenoid region, photoelectrons produced by irradiation with He I radiation enter a flight tube inside which the magnetic field strength is controlled by a magnetic shielding cage and a system of external correction coils. By this means the field is allowed to fall from 0.0 1T at the entrance to the flight tube to 0.001 T at the far end, where the electrons are detected with a microchannel plate and a phosphor screen. Energy analysis can be performed with a gold-coated tungsten mesh grid at the entrance to the flight tube. An example of the magnification obtainable, and the quality of the image, even at this early stage in development, is shown in figure 28, in which two superimposed grids have been imaged. In this case the image was formed by accepting all the electrons from the specimen, i.e. no energy selection was performed.

The potentialities of this new technique are evident, particularly if its operation can be extended into the soft X-ray region, so that one has in effect imaging in X.p.s. There are many fields of research that would benefit from the capability of obtaining chemical information from analysed areas very much smaller than those currently analysed in X.p.s. and u.p.s.

PHILOSOPHICAL TRANSACTIONS OF THE ROYAL SOCIETY A MATHEMATICAL, PHYSICAL & ENGINEERING SCIENCES

PHILOSOPHICAL TRANSACTIONS OF THE ROYAL SOCIETY A MATHEMATICAL, PHYSICAL & ENGINEERING SCIENCES

Downloaded from rsta.royalsocietypublishing.org

MATHEMATICAL, PHYSICAL & ENGINEERING SCIENCES
THE ROYAL SOCIETY A
PHILOSOPHICAL TRANSACTIONS OF

Ellipsometry

In this technique plane polarized light is specularly reflected from the surface of interest. Although most measurements use visible or near infrared light, for reasons of experimental convenience, in fact any radiation across the whole spectrum from ultraviolet to infrared could be used in principle. Again, the majority of experiments have been carried out at a chosen fixed

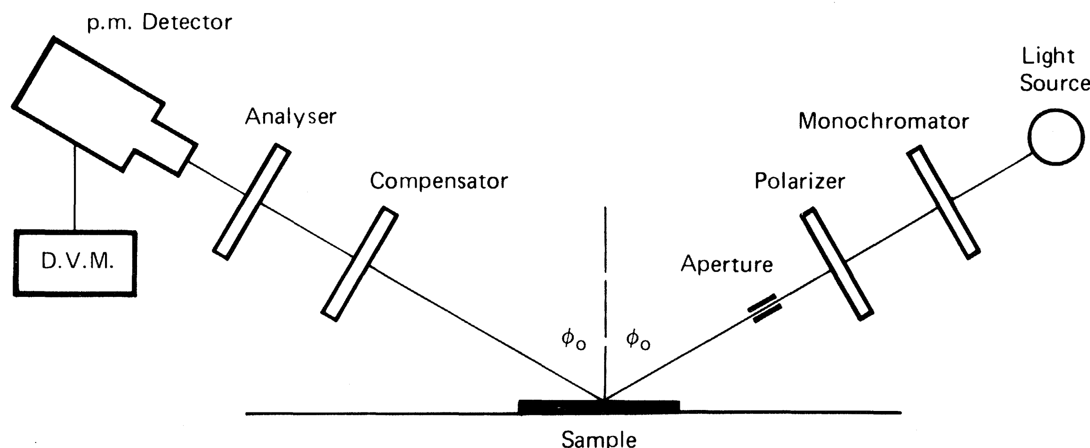

FIGURE 29. Basic experimental arrangement for measuring ellipsometric parameters, described by Neal (1979). Light from the source is monochromatized and polarized, appearing at the specimen surface as plane polarized light. After reflexion from the specimen its polarized state is generally that of elliptically polarized light. In the compensator it is converted to plane polarized light and can then be analysed in the analyser before detection in the photomultiplier.

wavelength, although there is more information to be gained by varying the wavelength continuously. After reflexion from the surface the optical constants of any film are determined from ellipticity of the reflected light, since no interfaces between two media of different dielectric properties are ever ideal, and in general the reflected light is not plane polarized but elliptically polarized. The parameters measured in practice are ψ and Δ, where tan ψ is the amplitude ratio of the resolved components of the electric vector of the incident light parallel to and perpendicular to the plane of incidence, and Δ is the phase difference of the two components. A basic experimental arrangement is shown in figure 29, from the review article by Neal (1979), which is recommended to the reader. Light from a source is wavelength-selected by a monochromator, polarized and reflected from the specimen. The reflected light is passed through a compensator, when it reverts to plane polarization, and can be analysed in an analyser followed by collection in a photomultiplier. Many variations on the basic arrangement are possible.

The power of ellipsometry lies in its ability to detect changes in optical properties corresponding to changes in film thickness of small fractions of a monolayer, and to do so in a completely non-destructive way, unlike, for example, A.e.s. or s.s.i.m.s. Aspnes (1980) has calculated that for incident light of wavelength 500 nm and a thin film of refractive index 1.5, the ultimate sensitivity in phase-shift measurement corresponds to a change in thickness of 5 pm. The technique is thus eminently suited to the following of surface reactions from the very earliest stages when initial adsorption on a clean surface occurs through to reactant layers several monolayers in thickness. In figure 30, an example from the work of Habraken *et al.* (1979), who have used ellipsometry extensively, the changes in Δ and ψ (expressed as $\delta\Delta$ and $\delta\psi$) are plotted against CO exposure on the same scale as the A.e.s. measurement of oxygen concentration. The copper

Downloaded from rsta.royalsocietypublishing.org

surface had previously been saturated with oxygen. From the A.e.s. observation it would be impossible to detect that any changes were taking place up to a CO exposure of *ca.* 1.5×10^5 L, but the linear variation in $\delta\Delta$ indicates that reaction is indeed proceeding. Oxygen is being removed from the surface, but is being replaced immediately by oxygen from beneath the surface. Eventually the supply of oxygen from underneath is depleted and all the measured

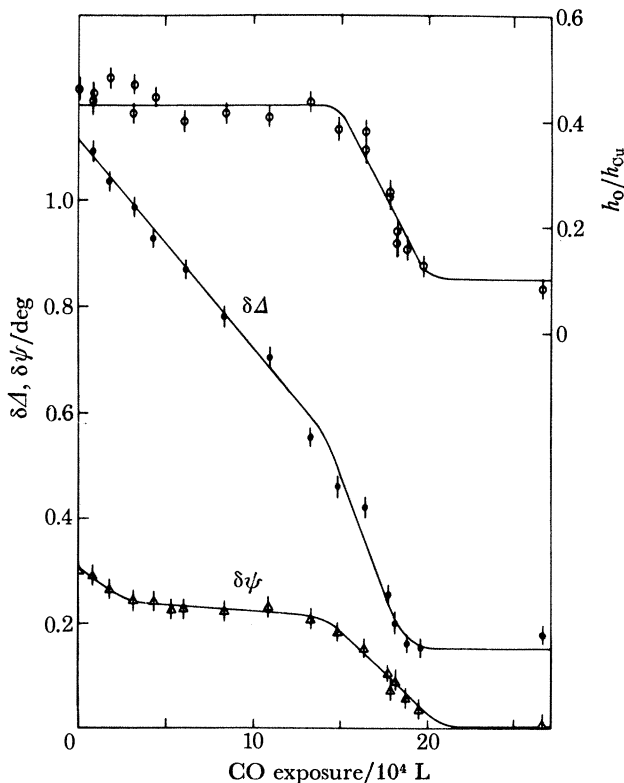

FIGURE 30. Use of ellipsometry by Habraken *et al.* (1979) in the study of the reaction of CO with oxygen adsorbed on a copper (111) surface at 207 °C. The left ordinate corresponds to changes in Δ and ψ (expressed as $\delta\Delta$ and $\delta\psi$) and the right ordinate to the related heights of the oxygen 512 eV and the copper 920 eV Auger peaks. Although the Auger ratio does not change up to exposures of 15×10^4 L, the continuous change in $\delta\Delta$ over the same region indicates that reaction is taking place. Beyond 15×10^4 L all the parameters change as oxygen is depleted in the subsurface layers.

parameters show changes; ellipsometry is therefore sensitive, in this particular experiment, to both surface and bulk oxygen, whereas A.e.s. is sensitive to surface oxygen only.

Ion excitation

Ion-excited Auger electron spectroscopy (*i.A.e.s.*)

Since the relaxation processes following the creation of a hole in a core level of an atom are independent of the method used to create that hole, it follows that a variety of spectroscopies are possible based on different methods of excitation, and on use of one or other of the relaxation paths. Electron and photon excitation, coupled with measurement of electron or photon emission, as the case may be, have already been described. Core hole ionization may also be caused

Downloaded from rsta.royalsocietypublishing.org

by ion excitation, and where the relaxation path chosen is that of the Auger process, the technique is known as ion-excited Auger electron spectroscopy (i.A.e.s.). (One can also, of course, choose the path of X-ray photon emission, in which case another technique, that of ion-excited X-rays, or i.e.X., is possible, but the very high ion energies needed for adequate X-ray production prevent i.e.X. from being surface-specific.)

In i.A.e.s. the exciting positive ions are normally those of argon, although other species have been used. A conventional ion gun, as employed on most surface analytical systems for specimen cleaning or for depth profiling, may also be used for the technique, but those workers interested

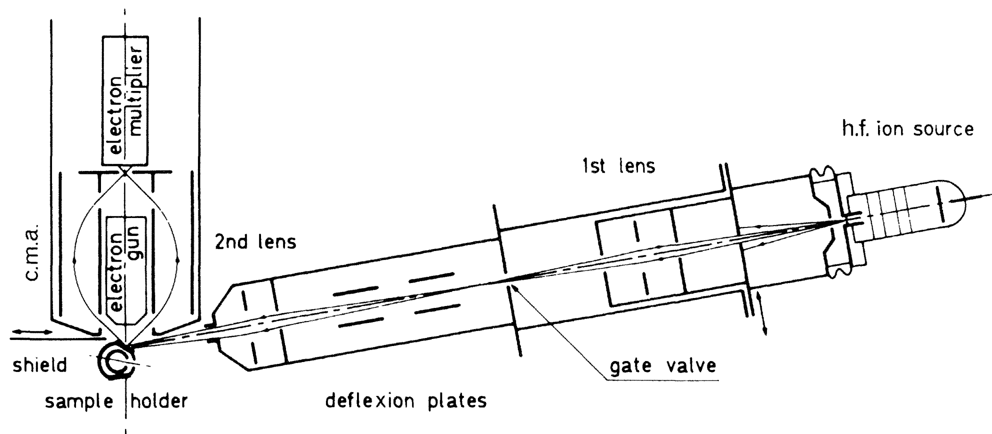

FIGURE 31. Experimental apparatus built by Viaris de Lesegno & Hennequin (1979) for the study of i.A.e.s. Primary ion beam conditions vary between 1 μA at 4 keV and 14 μA at 16 keV, into an area of 0.15 mm^2. Energy analysis is performed in a c.m.a., which also possesses a conventional coaxial electron gun for A.e.s. measurements.

in studying the basic physics of i.A.e.s. have often constructed special ion sources, as seen in figure 31, which is from Viaris de Lesegno & Hennequin (1979). The reasons for so doing are to permit a much greater range of ion energies and currents to be achieved than in the commercially available guns, and also smaller irradiated areas so that the ion beam can be rastered. The latter facility is essential for uniformity of the bombarded area. Figure 31 also emphasizes that surface analytical techniques are hardly ever employed singly but in combination, since conventional A.e.s. can also be performed on the specimen with an electron gun irradiating the same area as the ion gun.

Unlike A.e.s., i.A.e.s. has not been used extensively as an analytical tool, partly for historical reasons and partly because ion beam technology is more difficult than electron beam technology. There has also been the feeling that ion beam irradiation is inherently damaging to a surface, although there is now plenty of evidence about the damage that incident electrons can cause, too. Also, some of those very differences in the Auger spectra observed in A.e.s. and i.A.e.s. that have attracted workers wishing to study basic physical processes have tended to discourage the general application of i.A.e.s. Some of the differences are exemplified in figure 32, from Viel *et al.* (1976), in which the Auger spectrum of silicon produced by bombardment with 60 keV argon ions is shown; the spectrum is presented in both the direct and differentiated forms.

Comparison of the silicon spectrum in figure 32 with that obtained by A.e.s. would show immediately that superimposed on the rather broad $L_{2,3}VV$ peak is a very sharp peak that does not appear in A.e.s. Also there are two other additional peaks, marked P_1 and P_2, both sharp,

Downloaded from rsta.royalsocietypublishing.org

and separated from the major peak by energies too low (*ca.* 10 and *ca.* 20 eV, respectively) to be due to plasmon losses or multiples thereof. The interpretation by Viel *et al.* of the appearance of the major sharp peak is that of an Auger transition taking place in an atom or small cluster of atoms sputtered from the surface in an excited state, so that the transition is in fact 'quasi-atomic'. This would account for the unusual narrowness of the peak, and accounts also for the

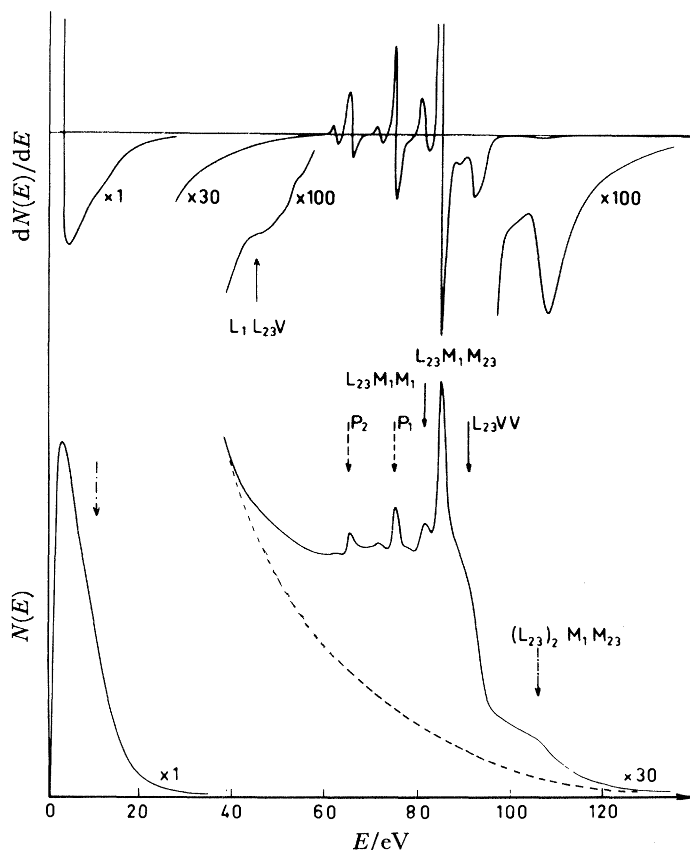

FIGURE 32. Auger spectrum excited from silicon by 60 keV argon ions, in the direct (lower) and differential (upper) modes. The assumed inelastic background is shown as a broken line under the lower spectrum. The ion-excited spectrum differs from the electron-excited one in the presence of the very sharp peak on top of the $L_{2,3}VV$ peak, interpreted as an Auger transition taking place in an atom in an excited state, sputtered from the surface. The peaks P_1 and P_2 then arise as losses from the sharp peak due to ionization of shallow atomic levels. (From Viel *et al.* (1976).)

existence of peaks P_1 and P_2, which would then arise by loss from the Auger peak of a quantity of energy (and its multiple) necessary to ionize a shallow quasi-atomic level in the sputtered atom, in this case the silicon M_1 level.

I.A.e.s. spectra are thus not quite as straightforward as those from A.e.s. in so far as they are not necessarily altogether characteristic of the solid state. On the other hand, it is clear that the technique might have some usefulness in the study of Auger spectra from excited atomic states.

Proton-excited Auger electron spectroscopy (p.A.e.s.)

Strictly speaking this technique is merely another aspect of i.A.e.s., but historically it has been treated separately since it often includes excitation by α-particles as well. In fact its development has been from the direction of the excitation of characteristic X-rays by heavy

PHILOSOPHICAL TRANSACTIONS OF THE ROYAL SOCIETY A MATHEMATICAL, PHYSICAL & ENGINEERING SCIENCES

PHILOSOPHICAL TRANSACTIONS OF THE ROYAL SOCIETY A MATHEMATICAL, PHYSICAL & ENGINEERING SCIENCES

Downloaded from rsta.royalsocietypublishing.org

ions, but since the fluorescence yield for light atoms is very small, attention has been turned instead to the Auger yield.

The instrumentation required for p.A.e.s. is more complex than for the other methods of excitation of Auger electrons, because of course the production of energetic protons and α-particles necessitates the use of a Van de Graaff generator as the primary source. An arrangement used by Kobayashi *et al.* (1976) is shown in figure 33; before entering the spectrometer chamber, the hydrogen or helium ion beams are passed through a charge exchanger for conversion to

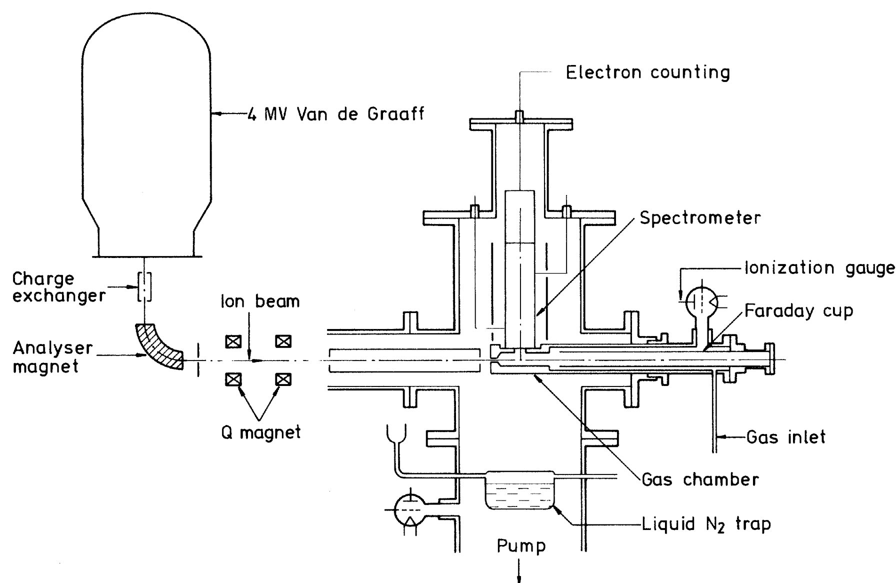

FIGURE 33. Experimental arrangement used by Kobayashi *et al.* (1976) for the excitation and analysis of Auger electrons by irradiation with protons and α-particles. Hydrogen and helium ion beams are produced in the Van de Graaff generator, then passed through a charge exchanger for conversion to protons and α-particles before being deflected and collimated into a narrow beam. The target in their study was a gas at high pressure. The primary energies used were between 0.3 and 2.6 MeV, and the primary currents between 0.1 and 1 μA.

proton or α-particle beams, respectively, and then deflected and focused into a collimated beam of diameter 2 mm. In this particular experiment the target was not a solid surface but a gas at relatively high pressure, so that Auger electron production was by ion–atom collisions, using a primary energy between 0.3 and 2.6 MeV and a primary current of 0.1–1.0 μA.

In figure 34, from the same paper, is shown a comparison of the Auger spectra of nitrogen excited in three different ways, by electrons, photons and α-particles. It can be seen at once that the latter two types of excitation produce much more fine structure than does electron excitation, and also that there are marked differences between proton and α-particle excitation. The peaks marked B, C and D are the so-called 'normal' lines, i.e. due to the $KL_{2,3}L_{2,3}$, $KL_1L_{2,3}$, and KL_1L_1 transitions, respectively, while those marked B′, C′, D′ are satellite lines. For α-particle excitation the satellite lines become comparable in intensity with the normal lines. The satellite A at energy higher than the normal line B is attributed to a transition involving a double ionization of the K shell, or in other words, a second electron excited state in coincidence with the first.

The satellite lines B′, C′ and D′ can be interpreted by being due to *simultaneous* ionization of the K and L shells of nitrogen, and their energies can be calculated and found to be in good

Downloaded from rsta.royalsocietypublishing.org

agreement with the production of multiple vacancies in the L shell. By using the electron-excited spectrum as a standard, the authors were able by successive subtraction to show that K ionization by protons and α-particles was accompanied by 40 and 90 % L ionization, respectively. By varying the primary energy, they were able also to derive the K shell ionization cross sections for proton and α-particle excitation for several light elements in addition to nitrogen. For proton excitation the observed cross sections followed the prediction of the Born theory closely, but for α-particle excitation there was considerable departure from the prediction. The latter

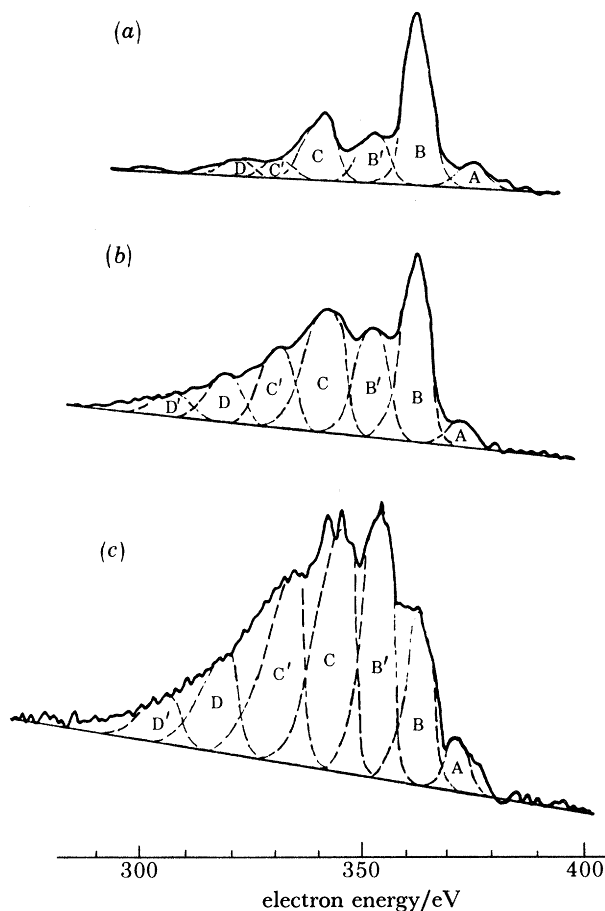

FIGURE 34. Comparison of the KLL Auger spectrum of nitrogen excited in three different ways, by (*a*) electrons at 2 keV, (*b*) protons at 1.0 MeV, and (*c*) α-particles at 1.6 MeV. The last two excitations produce much more fine structure than the first: in addition to the 'normal' lines B, C and D, there are the satellite lines B′, C′ and D′ arising from simultaneous ionization of both K and L shells. For α-particle excitation the satellite lines predominate, and it can be shown that in that case K shell ionization is accompanied by 90 % L shell ionization. (From Kobayashi *et al.* (1976).)

disagreement was said to be due to the screening effect of L electrons, since such a large proportion of L shell ionization was observed, and this effect would be larger for α-particles than for protons, being dependent on the effective nuclear charge.

Ion neutralization spectroscopy (*i.n.s.*)

When an excited or ionized atom arrives at a surface, an excited solid–atom 'couple' is formed, and ion neutralization is one of the paths of de-excitation of the excited system. It is in fact an Auger-type process, and depends on the juxtaposition of unfilled electronic levels in the

Downloaded from rsta.royalsocietypublishing.org

atom and filled electronic levels in the solid *at the surface*. The principle is illustrated schematically in figure 35 from Hagstrum (1970), who was the originator of the technique. On the left is the electronic energy level diagram of a metal, whose filled band stretches from the bottom B to the top F, the Fermi level, and on the right are two atomic wells, one of the He^{+} core and the other of the He^{2+} core. Where the atomic levels lie *within* the range of the filled band, de-excitation

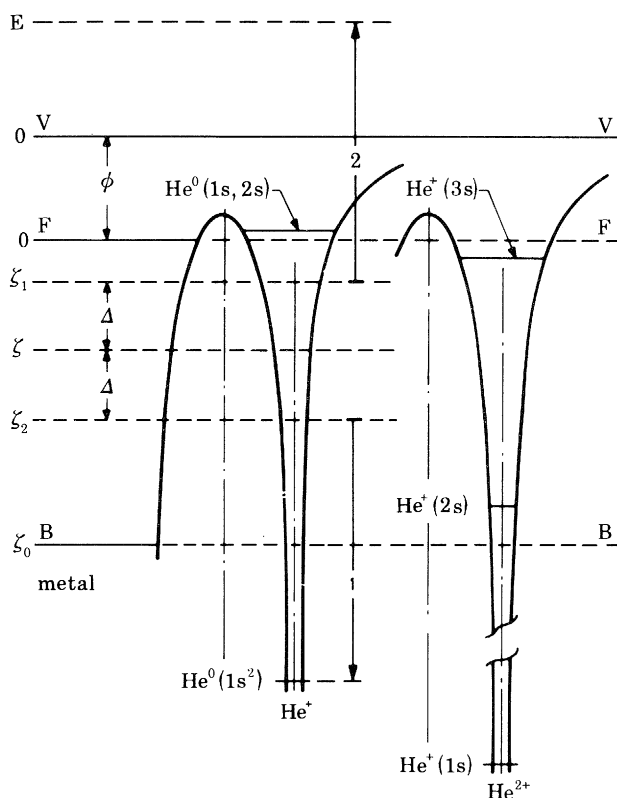

FIGURE 35. Schematic illustration of the principle of ion neutralization spectroscopy, according to Hagstrum (1970). If the atomic levels of an ion approaching a metal surface lie within the range of the filled band, i.e. B to F, as for the He^{2+} ion on the right, then de-excitation occurs simply by tunnelling. On the other hand, if the atomic levels lie outside the range of the filled band, as for the He^{+} ion in the middle, then de-excitation takes place by an Auger-type process exemplified by transitions 1 and 2. The levels ζ_1 and ζ_2 from which the electrons originate can be located anywhere within the band, so that an analysis of the ejected electron energies gives information about the local density of states.

can occur simply by tunnelling of electrons from the band into the empty atomic levels, and no information about the initial states of electrons in the filled band is available. If such information is desired, then the atomic levels must lie *outside* the range of the filled band, as for He^{+} in the example of figure 35, whereupon de-excitation can take place by Auger emission, shown as the transitions 1 and 2. The electrons taking part in the latter transitions are shown as originating in band levels ζ_1 and ζ_2, and since either of these levels could be located anywhere within the band the observed spectrum is obviously a convolution of the distribution of electronic levels in the filled band of the metal. The deconvolution of the spectra is a complex mathematical procedure that has been developed by Hagstrum, and will not be described here. It is sufficient to state that the end result is a transition–density function that includes both the density of states in the filled band and the transition probabilities for those states, and should therefore be comparable with, say, u.p.s. measurements. Note, however, the important point that because the

Downloaded from rsta.royalsocietypublishing.org

de-excitation in i.n.s. involves an atom actually *at* the surface, the density of states is characteristic of the surface itself and not of the bulk, whereas in X.p.s. and to a lesser extent in u.p.s. the valence band spectra relate more to bulk properties.

Although comparisons between i.n.s. transition–density functions and u.p.s. spectra for pure clean metals have been interesting, greater interest lies in the changes in the i.n.s. distributions

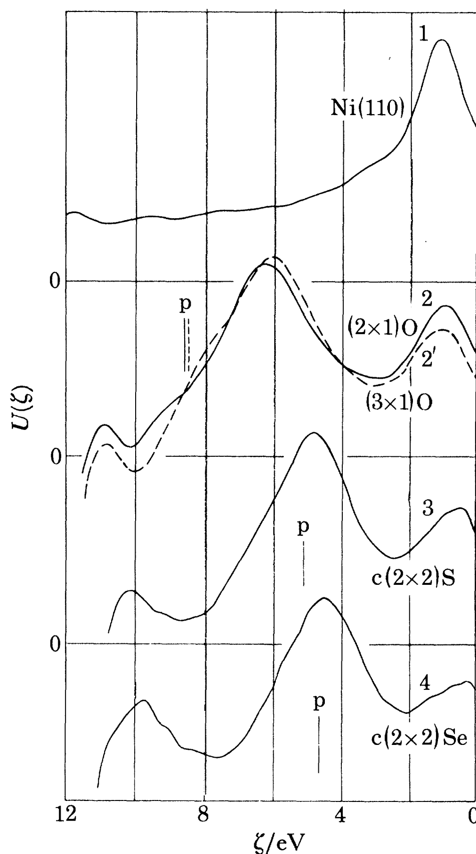

FIGURE 36. Transition–density functions obtained by Hagstrum (1970) using i.n.s., from nickel (110), clean and after reaction to produce adsorbed layers of O, S and Se. For sulphur and selenium the extra features below the d-band are in almost the same energetic positions as the p-orbital energies of the free atoms, but for oxygen there is a shift indicating a greater charge transfer to the adsorbed oxygen.

as a result of surface reaction. When atoms or molecules are adsorbed on a surface, then reaction produces a so-called 'surface molecule' in which the electronic orbitals may or may not be similar to those in the free atom or molecule. The energy spectra of these orbitals can be seen easily in i.n.s., as they can in u.p.s., and some examples are given in figure 36, from the work of Becker & Hagstrum (1972). At the top is the transition–density function for clean nickel in the (110) orientation, with the d-band peaking at *ca.* 1 eV below the Fermi level. The three curves below result from the adsorption of oxygen, sulphur and selenium, respectively, and in every case the magnitude of the d-band is reduced while extra structure appears a few electronvolts below the Fermi level. For sulphur and selenium adsorption the additional peaks correspond closely to the p-orbital energies of the free atoms (taking into account the work function of nickel) but for oxygen adsorption there is a shift of some 2.5 eV, indicating more negative charge on the adsorbed oxygen than on the sulphur or selenium.

Downloaded from rsta.royalsocietypublishing.org

Since transition–density functions such as those shown in figure 36 relate directly to the local density of filled states right at the surface, they are exactly what is required for the interpretation of the Auger spectra of adsorbate atoms involving valence electrons, and they have in fact been used in that way. Unfortunately i.n.s. is such a difficult and complex technique that it has been used very seldom apart from the work of Hagstrum, and so the data available from it are not nearly as extensive as one would like.

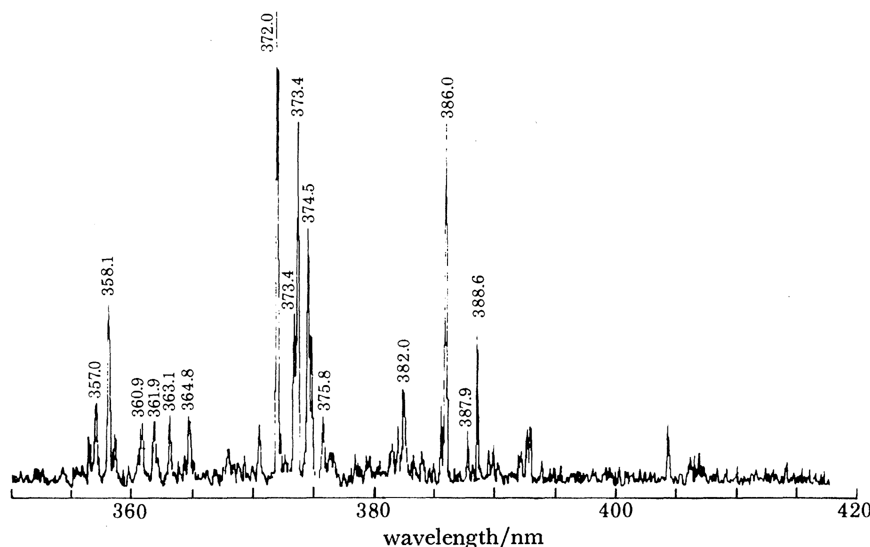

FIGURE 37. The Fe I emission spectrum observed by Martin & MacDonald (1977) as a result of bombardment of an iron surface by 50 keV argon ions. The spectrum closely resembles that from an arc discharge, implying that de-excitation of excited species leading to photon emission takes place in the gas phase away from the surface.

Ion beam spectrochemical analysis (*i.b.s.c.a.*)

The inelastic interaction of an ion beam with a solid surface can produce secondary electrons, Auger electrons, positive secondary ions, negative secondary ions, and excited neutrals. De-excitation or decay of ejected sputtered particles, be they ions or neutrals, can occur by a variety of processes, of which one is the emission of characteristic photons. The emission spectrum consists of a series of sharp lines, as seen in figure 37, which is from Martin & MacDonald (1977), and closely resembles that from an arc discharge, the implication being that de-excitation occurs in the gas phase away from the surface. Elemental identification can thus be made by reference to standard wavelength tables.

Incident ion energies between 5 and 50 keV are used, and current densities of the order of 100 μA cm^{-2}. Either inert (Ar^+) or reactive (O_2^+, N_2^+, etc.) bombardment can be used, although, as in s.s.i.m.s. (*q.v.*), the yields are generally increased with reactive ion species. An example of the dependence of photon intensity on oxygen partial pressure, for photon emission from pure chromium, is shown in figure 38, also from Martin & MacDonald (1977). All the Cr I lines go through a maximum in intensity at about the same partial pressure of oxygen, and it can be shown that the position of the maximum shifts to higher partial pressures as the primary ion current density increases, suggesting that the maximum is linked to the surface coverage of the chromium by oxide. The possibility thus arises of studying oxidation as a dynamic process, rather than in the more normal static situation where a surface is exposed to a certain dose of

Downloaded from rsta.royalsocietypublishing.org

oxygen and then analysed. As Martin & MacDonald point out, it is essential to carry out parallel s.s.i.m.s. measurements.

The behaviour of the Cr II emission line shown in figure 38 is more difficult to explain, since it would seem to be independent of the number of chromium atoms available in the surface. MacDonald & Martin (1977) suggest that the behaviour indicates a difference in the mechanism of ion and excited atom formation between clean and oxygenated surfaces, perhaps due to the blocking of electron exchange between oxygen and the metal when a different band structure, that of the oxide, forms at the surface. Clearly there is much yet to be learnt about the precise mechanisms of reactive ion enhanced photon (and ion) enhanced yields, and when a better understanding is gained so more information about surface reactions will be available.

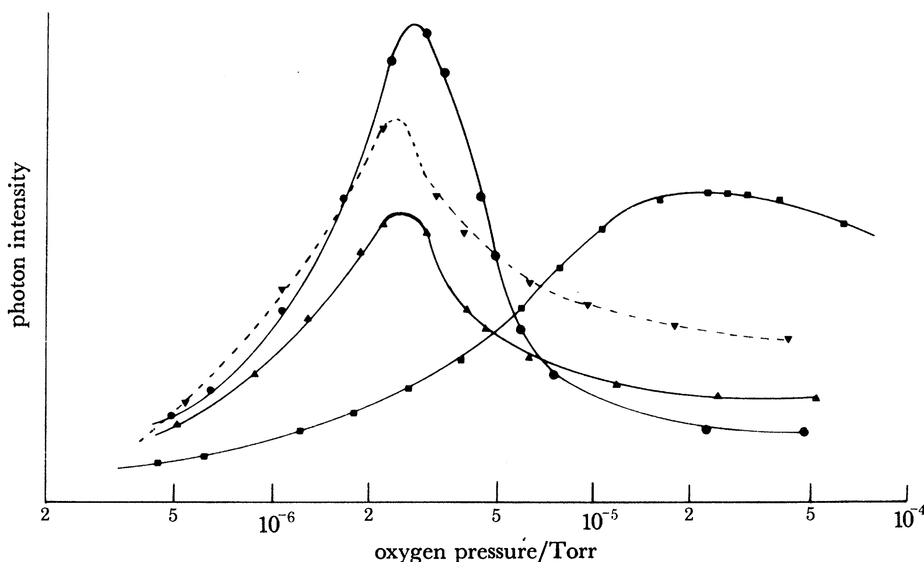

FIGURE 38. The effect on various chromium emission lines of the presence of oxygen at various pressures during the ion bombardment. All the Cr I lines (●, 425.4 nm; ▼, 404.9 nm; ▲, 302.1 nm) go through a maximum in intensity at the same partial pressure of oxygen; the position of the maximum can be shown to shift to higher pressures as the primary bombarding current increases. The behaviour of the Cr II line (■, 283.6 nm) is quite different and suggests a difference in the mechanism of ion and excited atom formation between clean and oxygenated surfaces. (From MacDonald & Martin (1977).)

Glow discharge optical spectroscopy (g.d.o.s.)

Unlike all the other techniques listed in table 1, the two glow discharge techniques g.d.o.s. and g.d.m.s. operate at high pressure, i.e. in the region 10 to 10^{-3} Torr. Nevertheless they are still surface-specific techniques since their information relates entirely to the sample surface; the major difference in their application compared with the others is that of course they cannot be used in surface physics experiments in which the starting point is either an atomically clean surface or a surface whose initial composition is well characterized. However, they have other advantages, as will be seen.

In both techniques the specimen is made the cathode in a diode-type discharge, but the design of the discharge cell differs according to whether emitted light or emitted ions are to be analysed. For g.d.o.s. the cell designed by Berneron & Charbonnier (1981) is shown in figure 39. The specimen, of diameter greater than 8 mm, is not only part of the cathode but also forms the vacuum seal against the cathode plate. With argon at pressures of a few torr admitted to the

Downloaded from rsta.royalsocietypublishing.org

cell, after prior evacuation to *ca.* 10^{-3} Torr, application of 1 keV d.c. between anode and cathode establishes a glow discharge from which argon ions bombard the specimen. Neutral atoms, which form the bulk of the sputtered material, are sputtered into the gas phase and are ionized or otherwise optically excited by exchange with excited argon species in the discharge. De-excitation occurs principally by emission of radiation characteristic of the specimen, and the light so emitted is first dispersed and then detected by photomultipliers, having passed through

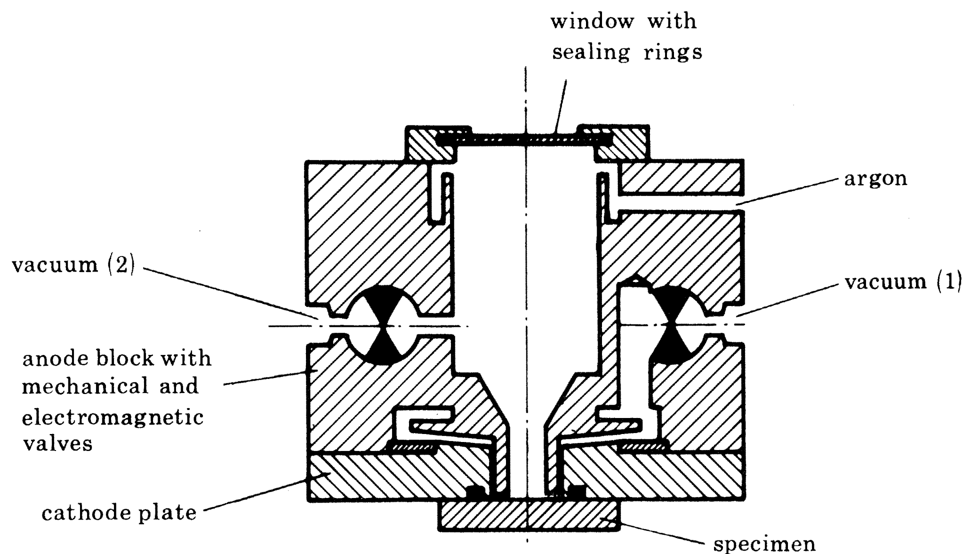

FIGURE 39. The cell designed by Berneron & Charbonnier (1981) for g.d.o.s. The specimen is sealed to the bottom of the cell via an O-ring and forms the cathode. With argon in the cell at a pressure of *ca.* 10^{-3} Torr, application of *ca.* 1 kV d.c. between anode and cathode establishes a glow discharge from which positive ions sputter the cathode. Neutral atoms sputtered into the cell space are ionized in the discharge, and de-excite by emission of visible photons that are then detected through the window.

a window immediately opposite the specimen. Although the sputtering rate is high, the speed and sensitivity of the analysing system are such that thin surface layers can easily be detected. Thus sputtering times of only a few seconds are sufficient for a depth analysis of several hundred nanometres, and therefore the specimen turn-around time is very short. Eventually the sputtered material depositing in the cell leads to short-circuits, necessitating removal of the deposits, and there is also the problem that the previously sputtered material might be re-sputtered, leading to memory effects.

An example of an application of g.d.o.s. from Berneron & Charbonnier (1981), is given in figure 40. Concentration profiles of nitrogen, oxygen and carbon have been obtained from iron surfaces nitrided in three different ways. Concentration calibration was achieved by using standards, and depth calibration by measuring the depth of the eroded crater with a profilometer. The scale in figure 40 corresponds to about 1 μm min^{-1}. The detection limits vary from about 0.001 % by mass for carbon to 0.1 % by mass for oxygen and nitrogen, the latter relative insensitivity being due to interference from background gases produced by desorption from the walls of the cell.

Static secondary ion mass spectrometry (s.s.i.m.s.)

As already mentioned in the description of i.b.s.c.a., interaction of an ion beam with a solid surface can involve several processes, leading to the emission of secondary electrons, secondary

Downloaded from rsta.royalsocietypublishing.org

ions or neutrals, as the case may be. Those techniques that are concerned with mass analysis of the secondary ions, positive or negative, fall under the general heading of secondary ion mass spectrometry (s.i.m.s.), but in the context of this article it is important to point out that according to the way s.i.m.s. is used, it may or may not be regarded as a surface-specific technique. Thus in *dynamic* s.i.m.s. the current density of the primary ion beam is kept high, of the order of

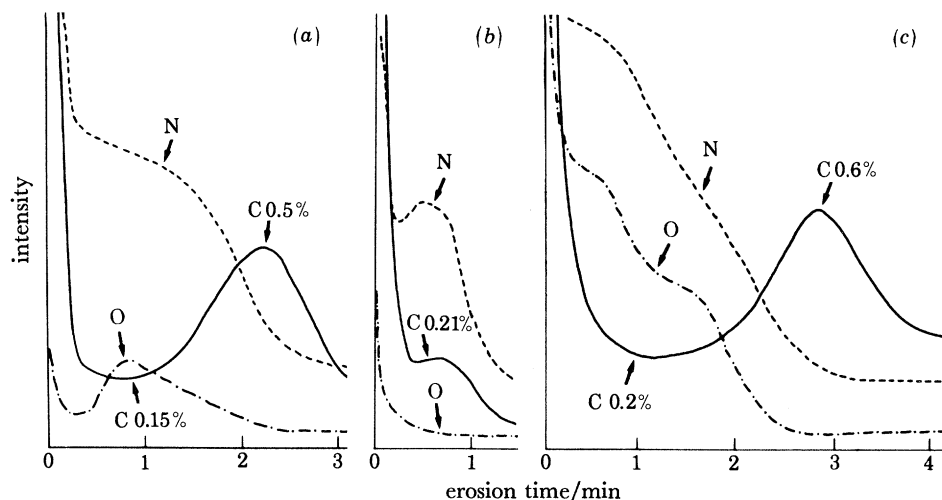

FIGURE 40. Concentration profiles by g.d.o.s. of iron surfaces that have been nitrided in three different ways: (*a*) gas nitrided; (*b*) ion nitrided; (*c*) salt bath nitrided. The erosion rate was 1 μm min^{-1}. (From Berneron & Charbonnier (1981).)

10^{-4} A cm^{-2}, so that the specimen is eroded at too rapid a rate for information about the original surface to be obtainable. In that version of s.i.m.s. the ion probe size is generally small, and the fast erosion allows sufficient intensity in any one mass signal for the specimen to be imaged by using that signal. It is basically a bulk rather than surface analytical technique.

If the primary ion current density is reduced by some orders of magnitude, to about 10^{-9} A cm^{-2}, the rate of erosion drops accordingly, and there is then sufficient time, by using a sensitive quadrupole mass spectrometer, to analyse the original surface and whatever was on it, before it is removed. Typically a monolayer would be removed in about 15 min. This version of s.i.m.s. is known as static secondary ion mass spectrometry (s.s.i.m.s.); the name is due to its originator, Benninghoven. Obviously the rate of arrival of contaminant atoms from the gas phase must be far lower than the rate of removal of surface atoms, so that very good vacuum conditions are required.

Both versions of s.i.m.s. provide information about the elements present on a surface, although it is still not easy to convert such information into percentage composition because of severe matrix effects, and also in principle about compounds present, since clusters of atoms as well as single atoms can be sputtered. An example of the latter capability is shown in figures 41 and 42, from Benninghoven (1973), in which the oxidation of clean silicon was studied by s.s.i.m.s. when the fraction of water vapour in the otherwise pure oxygen was kept below 10^{-4} then the negative ion spectrum of figure 41 was obtained, with only the atomic ion O^- and the cluster ions SiO_2^- and SiO_3^- observed. When the fraction of water vapour was allowed to rise above 10^{-3}, however, the spectrum changed markedly, as in figure 42, where now cluster ions characteristic of a proportion of hydroxide on the surface have appeared. Clearly the oxidation of clean silicon is very sensitive to water vapour contamination, but no technique other than s.s.i.m.s. with its

Downloaded from rsta.royalsocietypublishing.org

ability to detect ions containing hydrogen, and clusters characteristic of the surface compound, would have been able to establish the fact.

S.s.i.m.s. can be used continuously to follow the course of a surface reaction such as oxidation by monitoring both positive and negative secondary ion spectra. Benninghoven & Müller (1973) have studied many reactions in this way, and some of their results for the oxidation of chromium are shown in figure 43, in which some selected secondary ion yields are plotted against the

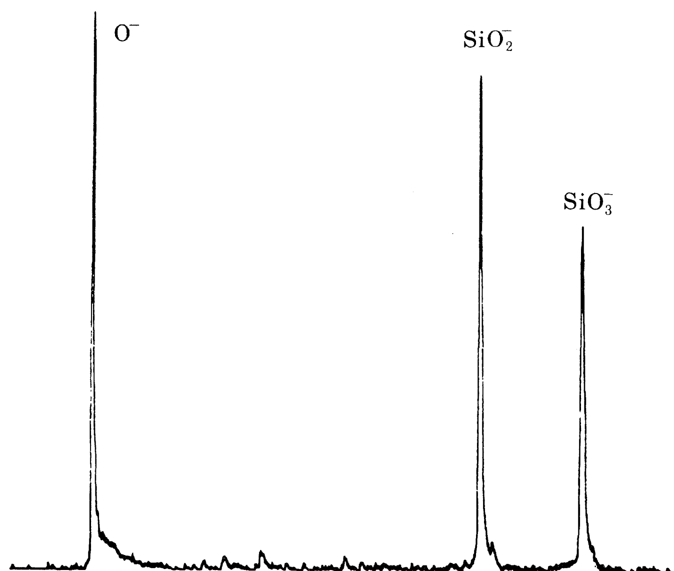

FIGURE 41. Negative secondary ion spectrum from a silicon surface after exposure to 1000 L of oxygen containing less than 10^{-4} fraction of water vapour. The oxide layer is characterized by the ions O^-, SiO_2^-, and SiO_3^-. (From Benninghoven (1973).)

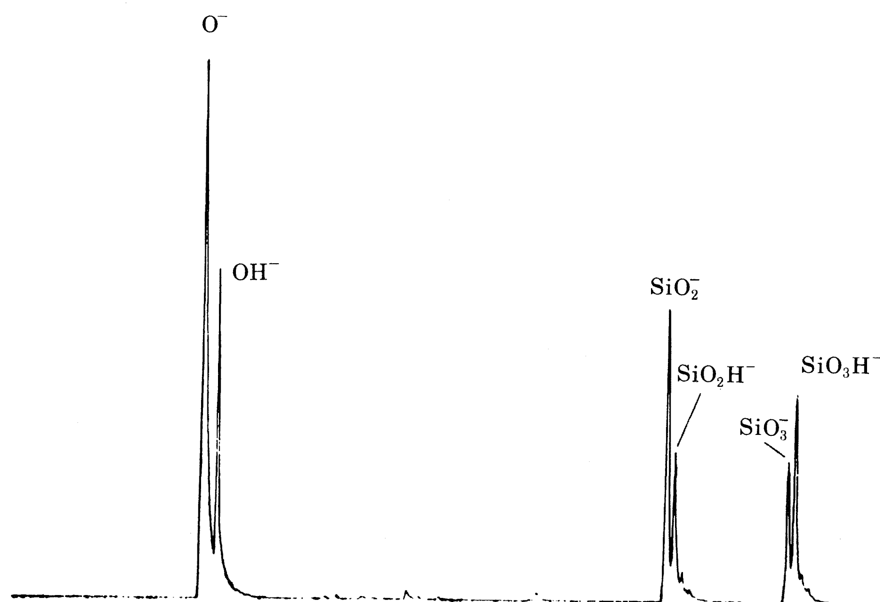

FIGURE 42. Negative secondary ion spectrum from a silicon surface after exposure to 1000 L of oxygen containing more than 10^{-3} fraction of water vapour. In contrast to the spectrum of figure 41, the secondary ions OH^-, SiO_2H^-, and SiO_3H^- now appear, indicating the sensitivity of the oxidation of silicon to the presence of small amounts of water vapour. (From Benninghoven (1973).)

Downloaded from rsta.royalsocietypublishing.org

oxygen dose. The principal deduction is that the initial oxide formed is characterized by, among others, CrO_2^- ions, but that as the oxide thickness increases, a second oxide phase characterized by CrO_3^- and CrO^+ grows over the first. The Cr_2^+ and Cr_3^+ yields decrease because of the decreasing probability of finding two or three uncombined chromium atoms adjacent on the surface as oxidation proceeds.

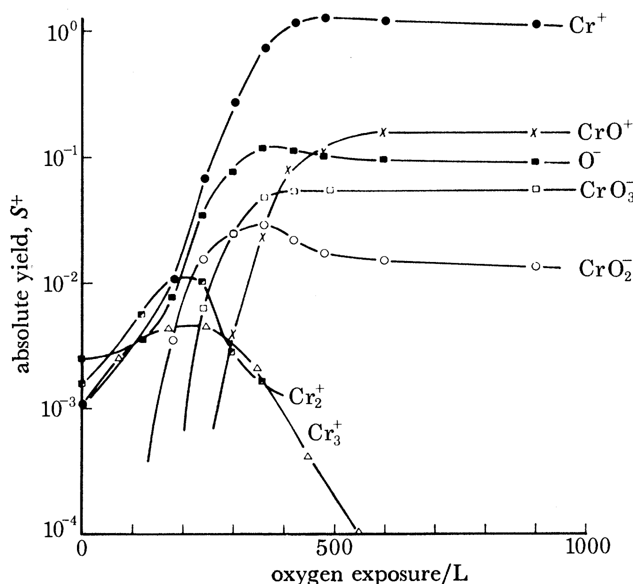

FIGURE 43. Absolute yields of some selected secondary ions during s.s.i.m.s. analysis of a chromium surface during oxidation in pure oxygen. The initial stage of oxidation is characterized by the ion CrO_2^-, whose yield goes through a maximum and then decreases as the yields of CrO_3^- and CrO^+ begin to increase. The latter ions are characteristic of the second oxide phase formed. The yields of Cr_2^+ and Cr_3^+ decrease below the limit of detection with increasing oxidation owing to the reducing probability of finding two or three uncombined chromium atoms adjacent in the surface. (From Benninghoven & Müller (1973).)

Ion-scattering spectroscopy (*i.s.s.*)

Since ions of an inert gas have a very strong electron affinity, there is a high probability that such ions will be neutralized after the first collision with atoms in a surface. After the second and third collisions the number of remaining ions will be negligibly small, although the proportion will vary with ion type and with angle of incidence. If, then, a beam of inert-gas ions is directed at a surface, and the mass analyser is set to detect the ions of the same mass and charge, it will analyse those primary ions that have been elastically scattered as a result of one collision only, i.e. from the outermost layer of atoms. Furthermore, if primary ions of low energy (e.g. 1–4 keV) are used, the elastic interaction time is much shorter than the Debye–Waller vibration time of a surface atom, so that the collision can be approximated to that between an ion of an inert gas and a free atom. Under those conditions there is a direct relation between the energy and mass of the primary ion on the one hand and the energy of the reflected ion on the other. For a scattering angle of 90°, the relation reduces to the simple form

$$E_r/E_p = (M_{at} - M_{ion})/(M_{at} + M_{ion}), \quad (2)$$

where E_r is the energy of the reflected ion, E_p the energy of the primary ion, M_{at} the mass of the surface atom and M_{ion} the mass of the primary ion.

Downloaded from rsta.royalsocietypublishing.org

This is the principle of ion-scattering spectroscopy (i.s.s.). From the foregoing description it will be realized that i.s.s. is the most surface-specific of all the techniques described here, since it is restricted in analysis entirely to the first layer of atoms. Confirmation of this specificity is given by figure 44, from Brongersma *et al.* (1974), in which i.s.s. spectra from a silicon surface before and after adsorption of a monolayer of bromine are recorded. One bromine atom adsorbs to each silicon atom, and the diameters of the bromine atoms are such that the bromine layer is just close-packed. After adsorption no silicon signal is detected.

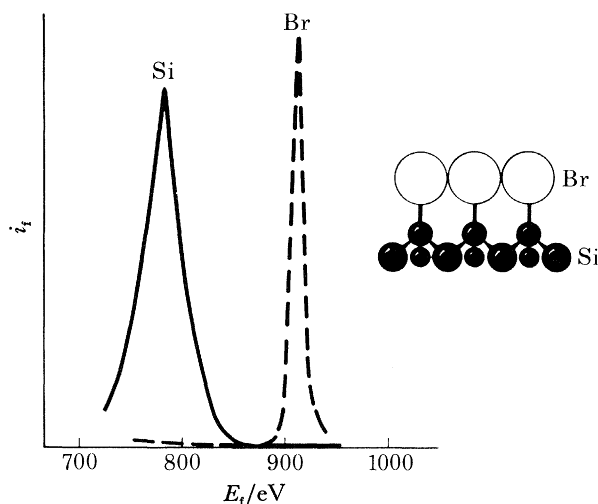

FIGURE 44

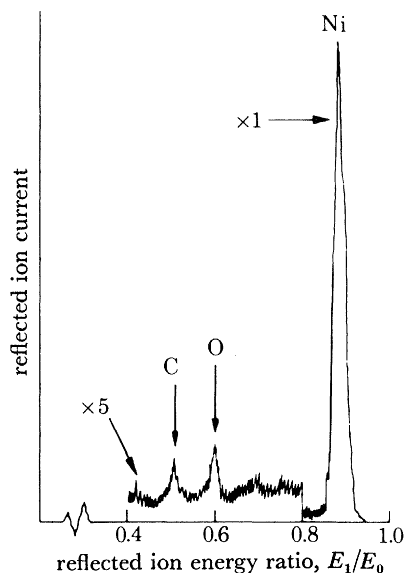

FIGURE 45

FIGURE 44. Demonstration by Brongersma *et al.* (1974) of the surface specificity of i.s.s. After adsorption of a layer of bromine onto a silicon surface, no signal due to silicon can be detected, only that due to bromine. One bromine atom adsorbs to each silicon atom in the surface, and the bromine ad-atoms then form a close-packed layer. Information has thus come only from the top layer.

FIGURE 45. Plot of elastically scattered ion current against the scattered ion energy ratio E_1/E_0 $(=E_r/E_p$ in (2)) from a nickel surface partly covered with carbon monoxide, showing the ability of i.s.s. to detect light elements on a surface with good resolution. The He^+ ion energy was 1.5 keV. (From Goff & Smith (1970).)

The primary ions most commonly used in i.s.s. are He^+, Ne^+ and Ar^+, and for any one experiment or material the ion and its energy are chosen to optimize the sensitivity or the mass resolution. Obviously no analysis can be obtained for surface atom masses lower than that of the primary ion, and also of course the resolution degrades with increasing difference between the masses of the ion and surface atom. However, care has to be taken in using primary ions of mass greater than He^+ because of the increased probability of surface erosion by sputtering.

The ability of i.s.s. to detect light elements on a surface, and hence to follow the course of many surface reactions, is demonstrated in figure 45, from Goff & Smith (1970), where adsorption of carbon monoxide to low coverage causes appearance of peaks due to carbon and oxygen. Although the resolution of mass for heavy elements is not as good as for light, some useful observations on surfaces containing heavy elements can still be made, as seen in figure 46, due to Nelson (1976), where the surface composition of a binary Ag–Au alloy is monitored as a function of temperature. The observed segregation of silver with increasing temperature has also

Downloaded from rsta.royalsocietypublishing.org

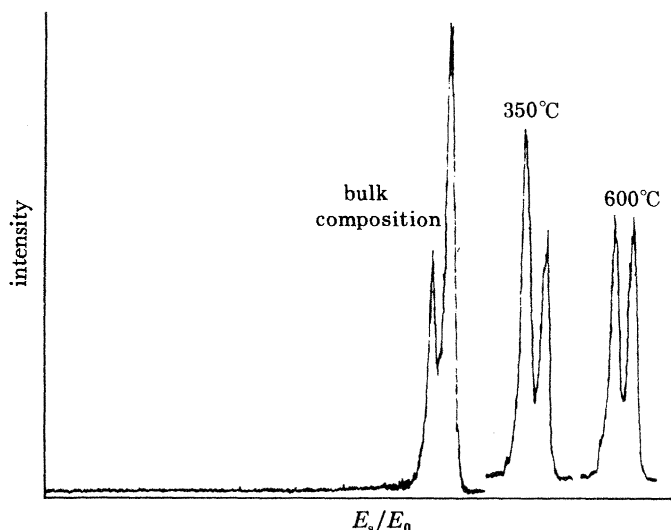

FIGURE 46. Plot of elastically scattered He^+ ion current against the scattered ion energy ratio E_s/E_0 (= E_r/E_p in (2)) from an Ag–Au alloy as a function of temperature. With increasing temperature there is first a considerable enhancement of the surface silver concentration due to segregation, and then the reverse process of solution in the gold as the temperature reaches 600 °C. The spectra show that for the heavy elements, with the use of light ions, the resolution in i.s.s. is not as good, but still usable. (From Nelson (1976).)

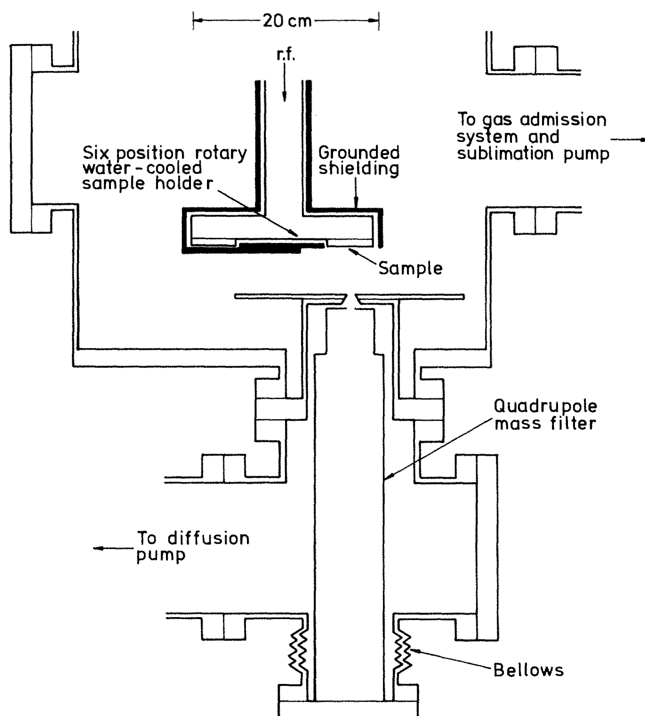

FIGURE 47. The system built by Coburn *et al.* (1974) for the application of g.d.m.s. as a surface analytical technique. Six specimens can be accommodated on the sample holder, which can be rotated to bring each specimen in succession behind a hole in a shield, so that only one specimen at a time is subject to sputtering. In that position the specimen is also opposite the orifice leading to the mass spectrometer. The discharge gas is purified by a titanium sublimation pump, thus minimizing the risk of specimen recontamination after sputtering.

Downloaded from rsta.royalsocietypublishing.org

been monitored by other techniques, such as A.e.s., but i.s.s. reveals that the enhancement of the silver concentration is even greater in the outer atomic layer than in the adjacent near-surface layers.

Glow discharge mass spectrometry (g.d.m.s.)

In the description of the g.d.o.s. technique some mention was made of g.d.m.s. because the two techniques are closely related. Whereas g.d.o.s. analyses the visible light emitted by de-excitation of excited neutrals in the discharge region above the specimen, g.d.m.s. analyses the

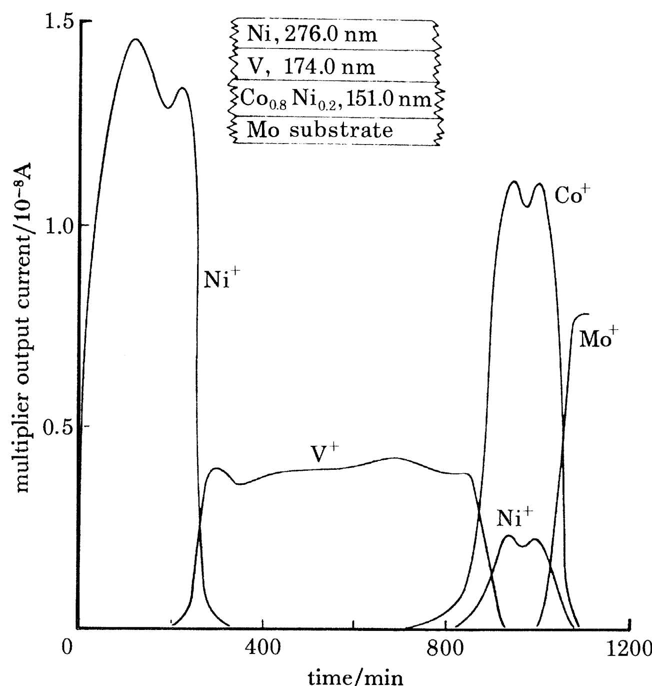

FIGURE 48. G.d.m.s. profile through the multilayer metal sandwich shown in the upper part of the figure. The various interfaces are of similar sharpness to that obtainable with combined A.e.s. and sputter profiling. The sensitivity for nickel in the pure nickel was found to be almost the same as for nickel in the alloy, indicating minimal matrix effects. The overall sputtering rate was about 0.6 nm min^{-1}, and the area sputtered about 1.6 cm^2. (From Coburn *et al.* (1974).)

masses of ionized neutral atoms by extraction into a relatively low-pressure (10^{-5} to 10^{-6} Torr) region and passage through a quadrupole mass spectrometer. It is important to realize the difference in analysis between g.d.m.s. and s.s.i.m.s.: in s.s.i.m.s. the secondary ions ejected from the surface by the primary ion beam are analysed for mass directly; in g.d.m.s. positive ions formed at the surface by the discharge cannot leave the surface because of the direction of the electric field, so that the positive ions whose masses are analysed are those formed in the discharge as a result of the ionization of neutrals leaving the surface. Since the bulk of the material sputtered from a surface is in the form of neutrals, it follows that g.d.m.s. has a higher sensitivity per incident ion than has s.s.i.m.s.

Clearly there is a relation between i.b.s.c.a. and g.d.o.s. on the one hand, and between s.s.i.m.s. and g.d.m.s. on the other. All these techniques employ analysis by means of the sputtering process; i.b.s.c.a. and g.d.o.s. both use optical emission as the analytical signal, while s.s.i.m.s. and g.d.m.s. both use mass spectrometry, but the ionization mechanisms in the respective pairs

PHILOSOPHICAL TRANSACTIONS OF THE ROYAL SOCIETY A MATHEMATICAL, PHYSICAL & ENGINEERING SCIENCES

PHILOSOPHICAL TRANSACTIONS OF THE ROYAL SOCIETY A MATHEMATICAL, PHYSICAL & ENGINEERING SCIENCES

Downloaded from rsta.royalsocietypublishing.org

are quite different. Direct ionization is used in i.b.s.c.a. and s.s.i.m.s., and Penning ionization in the gas phase by g.d.o.s. and g.d.m.s.

The g.d.m.s. system used by Coburn *et al.* (1974) is shown in figure 47. Specimens can be mounted six at a time on the rotary holder and brought in succession opposite the sampling orifice leading to the mass spectrometer. The discharge gas is purified before use by a titanium sublimation pump so that the chances of contamination of the specimen surface are smaller than with the g.d.o.s. cell shown in figure 39. In figure 48 an example is given of the analysis of a thin-film layer structure by g.d.m.s., from Coburn *et al.* (1974). The sharpness of the interfaces is similar to that achieved by conventional sputter profiling combined with simultaneous A.e.s. analysis. The absence of any pronounced matrix effects is demonstrated in this case by the observation that the sensitivity for the detection of nickel in the outer layer of pure nickel was almost identical to that for the detection of nickel in the cobalt–nickel alloy. This is in contrast to the situation in s.s.i.m.s., where there are pronounced matrix effects.

Resolution and sensitivity

The foregoing sections have described the principles of the techniques and some of their applications. The other types of information generally required concern the depth and spatial resolution available, the ultimate elemental sensitivity, and the range of sensitivities. These data have been gathered into table 2, in so far as they are known, but it should be realized that there are still areas of considerable uncertainty, especially in the elemental sensitivities.

Table 2. Volume of analysed region and elemental sensitivities

	volume of analysed region		elemental sensitivities	
technique	depth, monolayers	area/mm^2	detection limit (at. %)	sensitivity variation
A.e.s.	1–5	5×10^{-7} to 5×10^{-5}	0.1	< 10
s.A.m.	1–5	2×10^{-9} to 5×10^{-7}	0.1	< 10
e.e.l.s.	1	0.1–2	0.1	not known
a.p.s.	1–5	10–100	*ca.* 0.5	*ca.* 10^3
e.i.l.	1–2	1	1	not known
e.s.d.	1–2	5×10^{-7} to 5×10^{-5}	*ca.* 0.5	not known
X.p.s.	1–8	1–15	0.1	< 10
X.A.e.s.	1–5	1–15	0.1	< 10
s.r.p.s.	1–6	1–3	0.1	< 10
u.p.s.	1–6	5–10	0.1	< 10
p.e.s.m.	1–6	5×10^{-8} to 5×10^{-6}	0.1	< 10
ellipsometry	1–3	1–10	*ca.* 0.2	not known
i.A.e.s.	1–5	0.1–10	0.1	< 10
p.A.e.s.	1–5	3	0.1	< 10
i.n.s.	1	*ca.* 10	*ca.* 0.5	not known
i.b.s.c.a	1–5	0.1–10	*ca.* 10^{-4}	*ca.* 10
g.d.o.s.	1–5	30–100	10^{-6}	*ca.* 10
s.s.i.m.s.	1–5	0.1–10	10^{-4}	*ca.* 10^4
i.s.s.	1	0.5–5	0.5	*ca.* 50
g.d.m.s.	1–5	30–100	10^{-6}	*ca.* 10^2

Downloaded from rsta.royalsocietypublishing.org

Conclusions

Twenty techniques, and some variations on them, have been described, that provide surface analysis specific to the first few atom layers. These techniques can be classed according to the method of primary excitation used, and the information obtainable from them is in many cases complementary, so that it is generally desirable to use two or more together in the same system. When several techniques are able to use the same analyser (e.g. X.p.s., u.p.s., A.e.s., and i.s.s. for energy analysis) it is then possible to carry out a variety of analyses without altering the specimen position.

For purely compositional information X.p.s., A.e.s., s.A.m., i.s.s. and s.s.i.m.s. are the most frequently used, the choice between them being dependent on the nature of the problem. For high spatial resolution one would use A.e.s. or s.A.m. (s.s.i.m.s. will soon have such a capability too), for extreme surface specificity i.s.s., for high sensitivity for certain elements s.s.i.m.s., and for relative ease of quantification X.p.s. Less frequently used, although just as capable of providing compositional information, are i.b.s.c.a., g.d.o.s. and g.d.m.s. The variation of A.e.s. by using other excitations, i.e. X.a.e.s., i.A.e.s. and p.A.e.s., are also able to give such information, but are not generally used for that purpose; instead they have been employed to study various aspects of the physics of the Auger and related processes.

If information about the chemical states of elements at a surface, or about surface compounds that have been formed by reaction, or about the detailed nature of the bonding of reactants to a surface, is required, then there is a wide choice of technique. Again, X.p.s. is the most widely used because the so-called 'chemical shift' can give direct information about chemical state, and it can also be used for valence band study, although the latter is not so specific to the surface itself. U.p.s. is also common, and the valence band information obtainable from it has been essential in the elucidation of many reaction mechanisms. The difficult technique of e.e.l.s. gives information about changes in molecular vibration frequencies at surfaces that complements the u.p.s. data; in principle infrared spectroscopy should be able to give the same information, but in fact its application to surfaces and surface coverages of only a few monolayers is even more difficult than that of e.e.l.s. When it can be interpreted fully, s.s.i.m.s. should be able to say a great deal about the nature of surface compounds formed during reaction, and it is one of the very few surface-specific techniques that can provide analyses of hydrogen and hydrogen-containing species. The same can probably be said of i.b.s.c.a., g.d.o.s. and g.d.m.s., although in all their cases the direct relation between what is measured and what was originally on the surface seems rather more remote. Again there is chemical information available from e.i.l. and e.s.d., but for maximum effectiveness those techniques should always be used in conjunction with at least one other, and certainly with one of the compositional techniques. I.n.s. is in a class by itself, not only in being the least used of all the techniques described here, but in providing unique information about density of electronic states appropriate to the surface itself; only recently, by careful analysis of Auger line shapes, has comparable information started to become available.

References (Rivière)

Allen, G. C. & Wild, R. K. 1981 *Applic. surf. Sci.* **8**, 278–289.
Andersson, S., Hammarqvist, H. & Nyberg, C. 1974 *Rev. scient. Instrum.* **45**, 877–881.
Apai, G., Wehner, P. S., Stöhr, J., Williams, R. S. & Shirley, D. A. 1976 *Solid State Commun.* **20**, 1141–1145.
Aspnes, D. E. 1980 *Surf. Sci.* **101**, 84–98.
Backx, C., de Groot, C. P. M. & Biloen, P. 1980 *Applic. surf. Sci.* **6**, 256–272.

Downloaded from rsta.royalsocietypublishing.org

Bastasz, R., Colmenares, C. A. & Somorjai, G. A. 1978 *Surf. Sci.* **71**, 397-406.
Bauer, E. & Poppa, H. 1979 *Surf. Sci.* **88**, 31–64.
Beamson, G., Porter, H. Q. & Turner, D. W. 1981 *Nature, Lond.* **290**, 556–561.
Becker, G. E. & Hagstrum, H. D. 1972 *Surf. Sci.* **30**, 505–524.
Benninghoven, A. 1973 *Surf. Sci.* **35**, 427–457.
Benninghoven, A. & Müller, A. 1973 *Surf. Sci.* **39**, 416–426.
Berneron, R. & Charbonnier, J. C. 1981 *Surf. Interface Anal.* **3**, 134–141.
Brongersma, H. H., Meijer, F. & Werner, H. W. 1974 *Philips tech. Rev.* **34**, 357–369.
Coburn, J. W., Taglauer, E. & Kay, E. 1974 *J. appl. Phys.* **45**, 1779-1786.
Dylla, H. F., King, J. G. & Cardillo, M. J. 1978 *Surf. Sci.* **74**, 141–167.
Eastman, D. E. 1971 In *Electron spectroscopy* (*Proc. Int. Conf., Asilomar, California*), pp. 487–514. Amsterdam: North-Holland.
Evans, C. A., Jr & Blattner, R. J. 1978 *A. Rev. Mater. Sci.* **8**, 181–214.
Hagstrum, H. D. 1970 *J. Res. natn. Bur. Stand.* A **74**, 433–441.
Hedman, J., Klassen, M., Nilsson, R., Sorokina, M. F., Kljushnikov, O. I., Nemnonov, S. A., Trapeznikov, V. A. & Zyryanov, V. G. 1971 *Physica Scr.* **4**, 1–6.
Holloway, P. H. & McGuire, G. E. 1978 *Thin solid Films* **53**, 3–18.
Houston, J. E. & Park, R. L. 1971 *J. chem. Phys.* **55**, 4601–4606.
Kobayashi, N., Maeda, N., Hori, H. & Sakisaka, M. 1976 *J. phys. Soc. Japan* **40**, 1421–1429.
Larrabee, G. B. 1977 *Scanning Electron Microsc.* **1**, 639–650.
MacDonald, R. J. & Martin, P. J. 1977 *Surf. Sci.* **67**, 237–250.
Martin, P. J. & MacDonald, R. J. 1977 *Surf. Sci.* **62**, 551–566.
Morgan, A. E. & Werner, H. W. 1978 *Physica Scr.* **18**, 451–463.
Neal, W. E. J. 1979 *Applic. surf. Sci.* **2**, 445–501.
Nelson, G. C. 1976 *J. Colloid Interface Sci.* **55**, 289–296.
Nyberg, C. 1977 *Surf. Sci.* **65**, 389–398.
Powell, R. A. 1979 *Applic. surf. Sci.* **2**, 439–442.
Seah, M. P. & Dench, W. A. 1978 *Surf. Interface Anal.* **1**, 2–11.
Viaris de Lesegno, P. & Hennequin, J.-F. 1979 *Surf. Sci.* **80**, 656–662.
Viel, L., Benazeth, C. & Benazeth, N. 1976 *Surf. Sci.* **54**, 635–646.
Wagner, C. D. 1978 *J. Vac. Sci. Technol.* **15**, 518–523.
Weber, R. E. 1972 *J. Cryst. Growth* **17**, 352–353.
Weightman, P., Roberts, E. D. & Johnson, C. E. 1975 *J. Phys.* C **8**, 550–566.

PHILOSOPHICAL TRANSACTIONS OF THE ROYAL SOCIETY A MATHEMATICAL, PHYSICAL & ENGINEERING SCIENCES
PHILOSOPHICAL TRANSACTIONS OF THE ROYAL SOCIETY A MATHEMATICAL, PHYSICAL & ENGINEERING SCIENCES

Downloaded from rsta.royalsocietypublishing.org

PHILOSOPHICAL TRANSACTIONS OF THE ROYAL SOCIETY A MATHEMATICAL, PHYSICAL & ENGINEERING SCIENCES

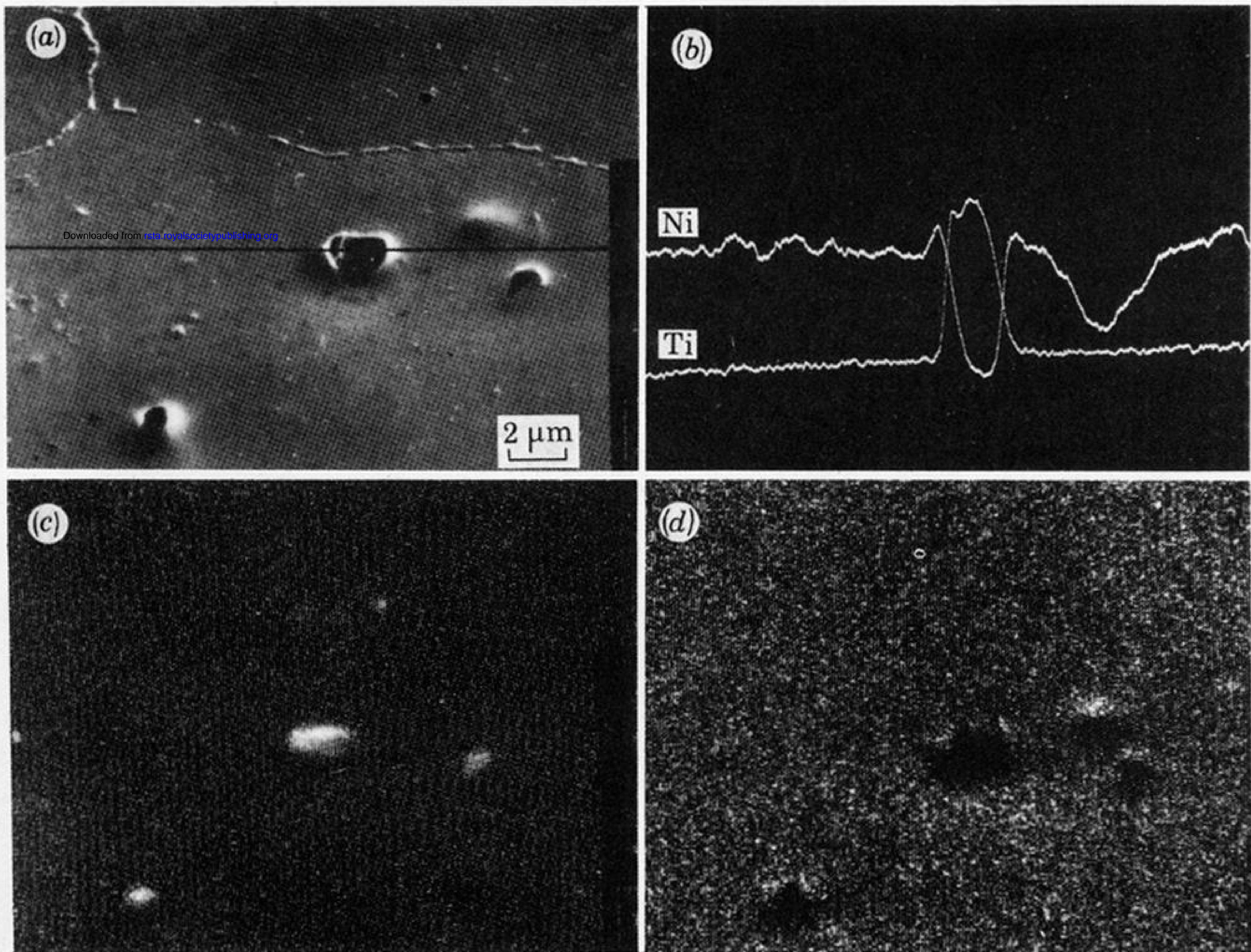

FIGURE 4. Analysis by s.A.m. of an inclusion in the surface of polished and etched Nimonic PE16. (*a*) Secondary electron image with line of analysis; (*b*) Auger line analysis through the inclusion, showing a deficiency of nickel and an excess of titanium, based on selected LMM peaks; (*c*) Auger map with the use of the titanium LMM signal; (*d*) Auger map with the use of the nickel LMM signal. Spot analyses of the inclusions confirmed that they consisted mostly of TiC. (From Mogami (1979).)

PHILOSOPHICAL TRANSACTIONS OF THE ROYAL SOCIETY A MATHEMATICAL, PHYSICAL & ENGINEERING SCIENCES

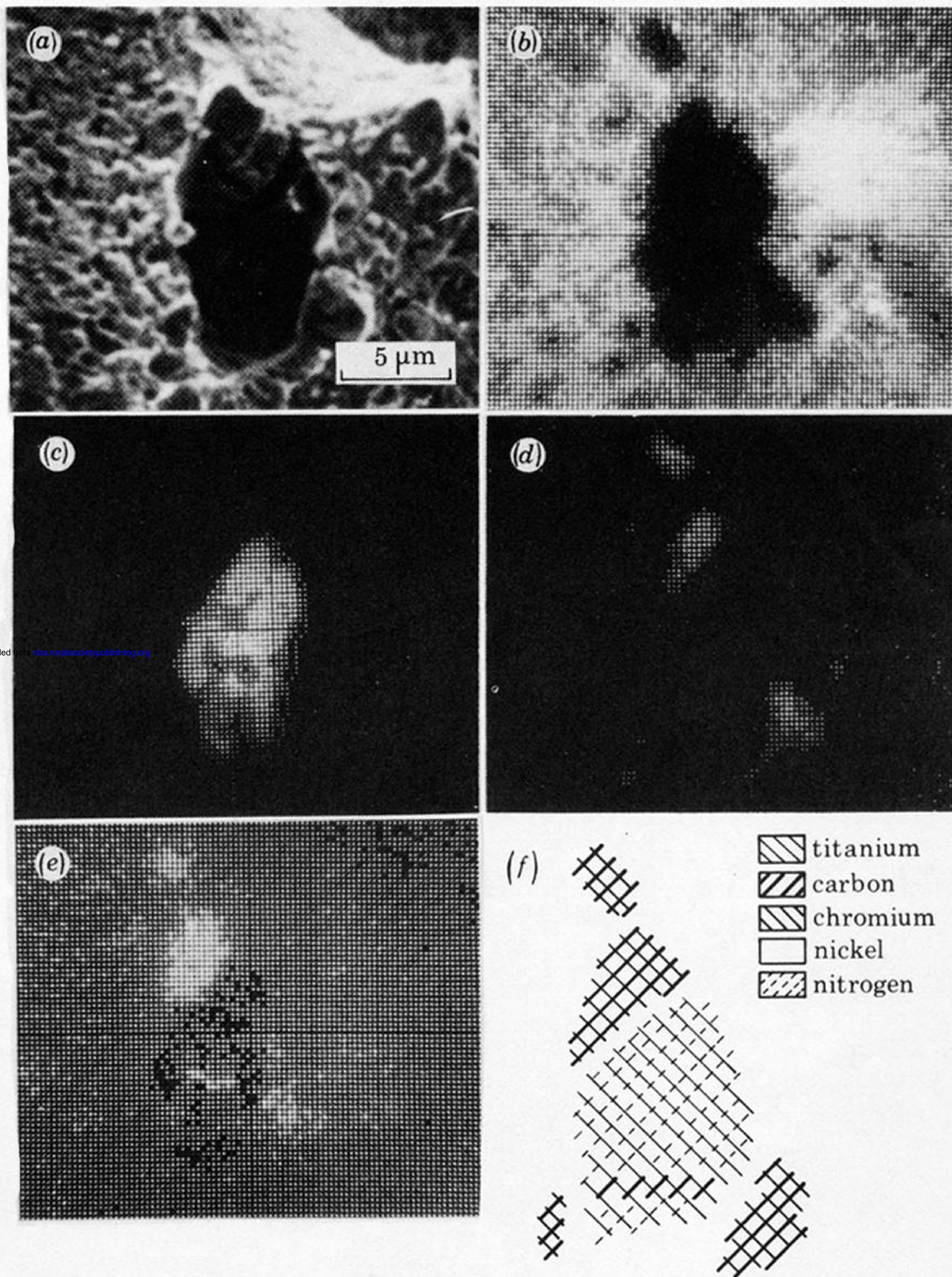

Downloaded from rsta.royalsocietypublishing.org

FIGURE 5. S.A.m. analysis of a particle found on the surface of a grain boundary exposed by intergranular fracture of a Nimonic 80A specimen: (*a*) secondary electron image; (*b*) Ni(836 eV); (*c*) Ti (373 eV); (*d*) Cr (518 eV); (*e*) C (272 eV). The maps have been computer enhanced to improve the contrast. Superposition of the maps gives (*f*), where it can be seen that part of the particle is chromium carbide, part titanium nitride, and the rest titanium carbide. (From Allen & Wild (1981).)

PHILOSOPHICAL TRANSACTIONS OF THE ROYAL SOCIETY A MATHEMATICAL, PHYSICAL & ENGINEERING SCIENCES
PHILOSOPHICAL TRANSACTIONS OF THE ROYAL SOCIETY A MATHEMATICAL, PHYSICAL & ENGINEERING SCIENCES

PHILOSOPHICAL TRANSACTIONS OF
MATHEMATICAL, PHYSICAL & ENGINEERING SCIENCES
THE ROYAL SOCIETY A
PHILOSOPHICAL TRANSACTIONS OF

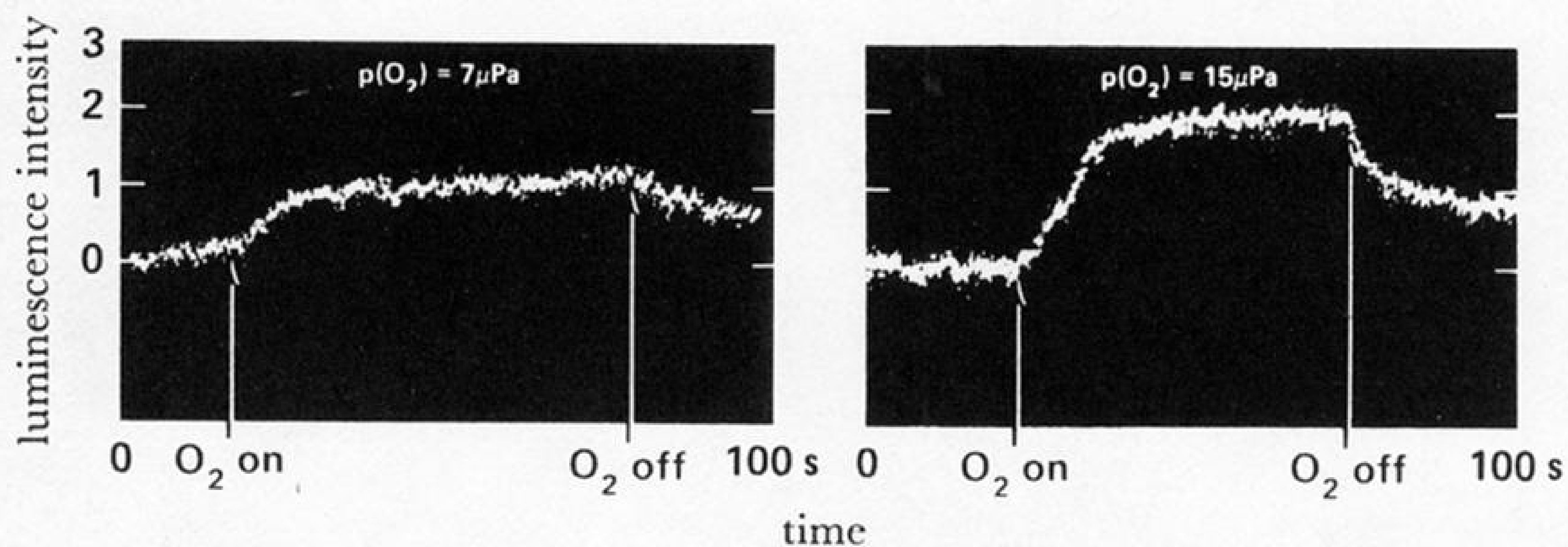

FIGURE 13. Variation in the e.i.l. intensity from a thorium specimen during exposure to oxygen. The intensity increased with oxygen admission until a plateau was reached; it remained there as long as the oxygen was present, and then decreased, but not to the original level, on removal of the oxygen. The level of the plateau reached during exposure was doubled when the partial pressure of oxygen was doubled. (From Bastasz *et al.* (1978).)

Downloaded from rsta.royalsocietypublishing.org

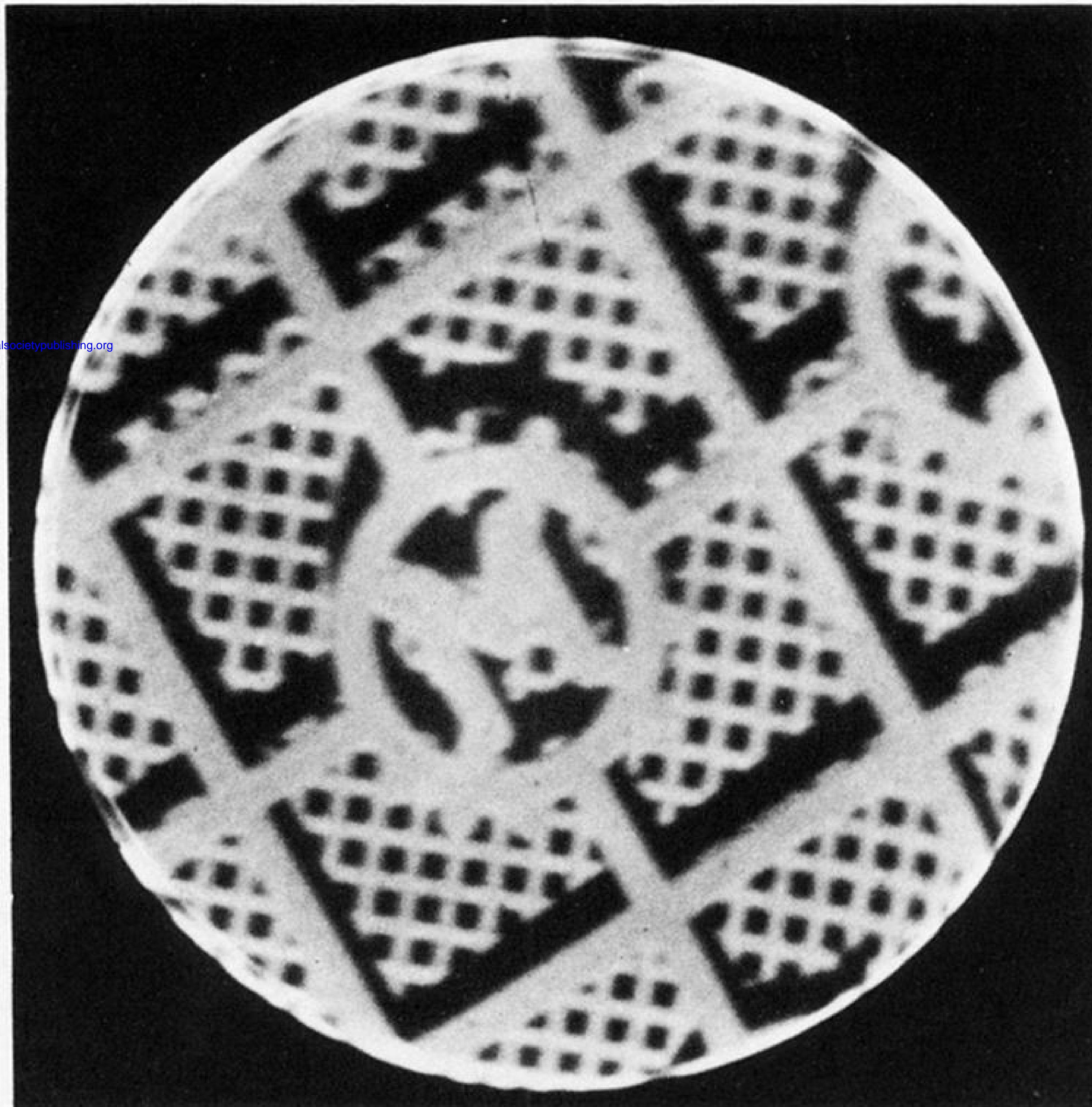

FIGURE 28. An example of the resolution obtained with the pre-production p.e.s.m. built by A. J. Dixon, K. A. Gehring & M. Keenlyside (personal communication 1982). The image is of two grids, a gold finder grid (with the letter M visible) on top of, but not in contact with, a 400 cm^{-1} mesh nickel grid. The spaces in the nickel mesh are about 18 μm, and the bars about 7 μm, in width. Shadows of the upper on the lower grid can be seen. The image was taken by He I photon illumination, and at a central magnetic field of 7.0 T. No energy selection was used, i.e. all photoelectrons were collected to form the image. (By courtesy of Thor Research Instruments, U.K.)

PHILOSOPHICAL TRANSACTIONS OF THE ROYAL SOCIETY A MATHEMATICAL, PHYSICAL & ENGINEERING SCIENCES

PHILOSOPHICAL TRANSACTIONS OF THE ROYAL SOCIETY A MATHEMATICAL, PHYSICAL & ENGINEERING SCIENCES